Resonance Trapping in Protoplanetary Discs

Aaron Lee [1]
Advisor: Fred Rasio[2]

May 11, 2007

[1]a-lee-1@northwestern.edu
[2]rasio@northwestern.edu

Contents

1 Introduction and Motivation **1**
1.1 Introduction 1
1.2 Detection Methods 2
1.3 Statistical Properties of Observed Systems 6

2 Physical Processes in Discs **10**
2.1 Planet Formation 10
2.2 Tidal Interactions 12
2.3 Review of Previous Work 16
2.4 Outline of Thesis 18

3 Numerical Setup: *ResCap* **20**
3.1 Runge-Kutta Method 20
3.2 Set-Up 24
3.3 Initial Tests 30
3.4 Migration 37

4 Results **39**
4.1 Migration and Eccentricity Damping 39
4.2 Can Eccentricity Save Planets? 45
4.3 Mass Limits on Resonance Trapping 47
4.4 Dynamical Instability: A Way to Make Eccentric Planets? 50

5 Summary and Discussion **55**

A List of Notation **58**

B *ResCap* Source Code **61**

References **62**

Chapter 1

Introduction and Motivation

1.1 Introduction

We have recently celebrated the tenth anniversary of the discovery of the first extrasolar planet around a solar-type star. What was shocking about the detection of this 0.5 M_J planet[1] (Mayor & Queloz 1995) was not that it was around a star like our Sun, but that the period of the planet, 51 Pegasi b, was measured to be only four days (for comparison, even Mercury's period around the Sun is several months). Its semi-major axis is 100 times smaller than Jupiter's around our Sun. At such distances, the planet is exposed to temperatures so high that the material needed to assemble the core cannot be found in a solid phase. The implication is that the planet formed much farther out and migrated inward. It was theorized that tidal interactions between the planet and the protoplanetary disc–the disc surrounding young stars where we believe form planets–can lead to orbital migration (Goldreich & Tremaine 1979, 1980; Lin & Papaloizou 1979, 1993). The theory had been developed about 15 years before the discovery of 51 Pegasi b, and this migration had been predicted. What was not predicted, however, was that planets of this size could be found on such short period orbits.

Today, there are over 200 known extrasolar planets in over 190 planetary systems (with systems housing as many as six planets).[2] Their orbital characteristics include systems with highly eccentric orbits and planets locked in mean-motion resonance. Past theoretical models have relied on the solar system for guidance, but it is now clear that there is a greater variety than ever imagined. These systems suggest that planet-disc tidal interactions are very important in determining the characteristics of planetary systems, and that the characteristics of the disc could have large implications on the system's final outcome. The study of extrasolar planets and their interactions with the

[1] In this paper, M_J will denote a Jupiter-mass, and M_E will denote an Earth-mass.
[2] See Jean Schneider's website: http://exoplanet.eu/ for a continuously updated list.

protoplanetary disc addresses significant problems regarding both the origin of planetary systems as well as conditions pertaining to the development of life both inside and outside our Solar System. By understanding how planetary systems form, we may better understand whether our Solar System might be unique in certain ways.

This thesis is organized as follows: In the remainder of this chapter, we will review the current methods and limitations of observing extrasolar planets and review the statistical properties of the observed systems. The second chapter is dedicated to describing the physical processes that take place during planet formation, including disc-planet interactions, orbital migration, and resonance trapping. Additionally, it summarizes previous studies that have been done on resonances in protoplanetary discs, and the goals of this work on resonances in protoplanetary discs. The third chapter describes my N-body integrator code, *ResCap*, developed to study resonance trapping phenomena. Additionally, I describe the set-up of my numerical integrations. The fourth chapter details the results obtained to date. Finally, in the fifth section, we consider the implications of this study for the understanding of the early evolution of planetary systems.

1.2 Detection Methods

1.2.1 Radial Velocity

Presently, almost all planets have been detected by the radial velocity technique, which consists of measuring the Doppler shift due to the motion of the star around the center of mass of the system, observing the influence orbiting bodies (planets) have on their host star. This measurement gives the velocity component projected along our line of sight, and is given as $v = K \cdot g(t)$, where $g(t)$ varies periodically with time t around the orbit and has a mean value of zero. For a one-planet system, $g(t)$ is of the form

$$g(t) = \cos(f(t) + \omega) + e\cos(\omega), \tag{1.1}$$

where f is the planet's true anomaly, ω is the argument of pericenter, and e is the orbital eccentricity.[3] The amplitude K can be easily derived using Kepler's third law and Newton's law of gravitation. For a planet of mass M_p orbiting a star of mass M_*, K is given by

$$K = \left(\frac{2\pi G}{T}\right)^{1/3} \frac{M_p \sin i}{(M_p + M_*)^{2/3}} \frac{1}{\sqrt{1-e^2}}. \tag{1.2}$$

Here, G is the gravitational constant, T is the orbital period of the planet, and i is the angle of inclination.[4] By measuring v, we can determine both the orbital period and the eccentricity. A Fourier transform can then be applied to the

[3] See Appendix A for a detailed description of each orbital parameter.
[4] An orbit viewed edge-on corresponds to $i = 90°$.

radial velocity curve to isolate the individual orbits of multi-planet systems. For a circular orbit ($e = 0$), $g(t)$ reduces to a sinusoid with unit amplitude. For non-circular orbits, $g(t)$ reaches an amplitude of $1 + e$ and, by measuring its departure from a sinusoid, we can determine the eccentricity e.

Radial velocity curves only give the components along our line of sight, and therefore, the inclination angle cannot be measured directly. Using Kepler's third law,

$$T^2 = \frac{4\pi^2 a^3}{G(M_* + M_p)} \approx \frac{4\pi^2 a^3}{GM_*}, \tag{1.3}$$

where I have assumed $M_p << M_*$, the radial velocity measurement can only provide a lower limit on the planetary mass by fixing the value of the projected mass $M_p \sin i$. However, for the population of the first 150 discovered objects, the ratio of the real mass to the projected mass is, on average, of order unity. Upper limits can be placed by requiring additional characteristics of the system, such as requiring that the system remain stable on timescales relative to the lifetime of the star. This generally provides a maximum i since systems tend to be more unstable with increasing planetary masses. Because forces increase with larger masses and smaller distances, larger planets close to the star are easier to detect through a radial velocity curve. Assuming that $M_p << M_*$, let us rewrite the expression for K and T as the following:

$$\begin{aligned} K(\mathrm{ms}^{-1}) &= 28.4 \left(\frac{T}{1\ \mathrm{yr}}\right)^{-1/3} \left(\frac{M_p \sin i}{M_j}\right) \left(\frac{M_*}{M_\odot}\right)^{-2/3} \frac{1}{\sqrt{1-e^2}}, \\ T(\mathrm{yr}) &= \left(\frac{a}{1\ \mathrm{AU}}\right)^{3/2} \left(\frac{M_*}{M_\odot}\right)^{-1/2}. \end{aligned} \tag{1.4}$$

The detection limit of current instruments is about $1\,\mathrm{m\,s^{-1}}$. The following table lists some particular maximum values of detectable distance for a solar star. They are determined from Equations 1.4, by equating $K = 1\ \mathrm{m\,s^{-1}}$ and solving for a. I then calculate the period the planet would have for a given semi-major axis.

$M_* = 1\ M_\odot$, $e = 0$, $i = 90°$		
M_p (M_J)	a_{max} (AU)	T_{max} (yr)
1	806.56	22906.3
0.5	201.64	2863.29
0.1	8.0656	22.9063
0.01	0.0806	0.0229
Earth	0.007976	0.007123

Table 1.1: Maximum Detection Distances

It is clear that Jupiter-size planets could be detected very far from their parent star, but radial measurements rely on the fact that multiple periods must be observed. This leads to a bias in radial velocity measurement, in that

massive planets with very short orbits are more easily detected. Additionally, this approach is far from detecting Earth-like planets anywhere close to the habitable zone, the distance from the star where water can exist in liquid form.[5]

1.2.2 Transits

A transit occurs when a planet passes in front of the star along our line of sight. We can then measure the relative change in the stellar flux of the star during the transit,

$$\frac{\Delta F_*}{F_*} = \left(\frac{R_p}{R_*}\right)^2, \tag{1.5}$$

coupled with the radial velocity measurements to greatly constrain the planet's mass[6] and determine the planet's radius. However, transits are not common, and only 19 have been detected to date. The probability of detecting a transit, R_*/a_p, for a $R_* = 1\ R_\odot$ star is only 10% with $a = 0.05$ AU, the smallest orbit known.

The first transiting planet (HD 209458 b) was observed in September 1999 by Charbonneau et al. (2000).[7] Transiting allowed us to determine HD 209458 b to have a mass of 0.63 M_J with a radius of 1.3 that the radius of Jupiter. This predicts a mean density of 400 $\mathrm{kg\,m^{-3}}$, significantly smaller than the density of Saturn (700 $\mathrm{kg\,m^{-3}}$), which is the least dense planet of our Solar system. This suggests that the planet consists primarily of gas, and it has been suggested that at such short distances, the atmosphere of the planet is evaporating (Vidal-Madjar et al. 2003, 2004)!

1.2.3 Astrometry

While the radial velocity method measures the motion of the star *along* the line of sight, it is also possible to measure the motion of the star *perpendicular* to the line of sight. For a circular orbit, the angular motion of the star is

$$\alpha(\mathrm{arcsec}) = \frac{M_p}{M_*}\frac{a/1\ \mathrm{AU}}{d/1\ \mathrm{pc}}, \tag{1.6}$$

where d is the distance to the star measured in parsecs. Since d and M_* are known, and a is given by the periodicity of the star's motion, M_p can be determined by measuring α. For comparison, the motion of the Sun from a distance of 10 pc due to Jupiter is 500 μas, whereas due to Earth from the same distance it is only 0.3 μas. From the ground, the best accuracy comes from inferometers, and VLTI and KECK expect to reach astrometric accuracies of 10 μas

[5] For the interested reader, to detect an Earth-size planet at 1 AU, this would require that we be able to measure amplitudes of 0.0893 $\mathrm{ms^{-1}}$. It is not clear if such precision could be reached, since it would have to be extracted from the intrinsic "noise" at the stellar surface, i.e. random Doppler shifts due to atmospheric oscillations, spots, or magnetic cycles.

[6] Since $\sin i$ must be close to 1.

[7] This was not the first planet detected using the transit method. The first planet detected by transit was TrES-1 by Alonso et al. in 2004.

in the near future. Currently developing space observations include the Space Interferometry Mission (SIM), and will have accuracies of order 1 μas. SIM is expected to be launched by NASA in 2010. Since stars being viewed are at least a few parsecs away, it will not be possible to detect terrestrial planets in habitable zones with this method, which is better suited for detecting giant planets. However, these measurements are easier for longer period systems, as compared to radial velocity measurements.

1.2.4 Microlensing

Gravitational microlensing requires a background star to provide a source of light, allowing the foreground star to act a gravitational lens when it passes in front of the background star, making the background star appear up to $\sim$1000 times as bright. A microlensing process typically lasts for several months. However, when the foreground star has a close companion, there can be two successive spikes of brightness superimposed on the regular light curve pattern of the microlensing event (Mao & Paczynski 1991, Gould & Loeb 1992, Bennet & Rhie 1996). This is most sensitive for planets within five AU of the lensing star, and planets less than an Earth mass can produce large effects on the light curves. This technique is well suited for finding terrestrial planets in habitable zones. However, microlensing patterns do not repeat, so follow-up monitoring must occur as soon as detections are made.

Four planets have been found by microlensing, with the first discovered in 2004 (Bond et al.), located 5.2 kpc from Earth. At these distances, radial velocity measurements would be useless. The detected planet has a mass and semi-major axis of 2 M_J and 3 AU, respectively.

1.2.5 Direct Imaging

The IR detection of the transiting planet HD 209458 b through a secondary eclipse (Deming et al. 2005) was the very first observation of photons emitted by extrasolar planets. It was done by observing the decrement in infrared flux when the planet passed behind its parent star. By measuring ΔF, a characteristic wavelength can be determined, and by assuming some model for the atmosphere of the planet, a blackbody temperature can be estimated.

This method will allow for long period objects to be detected, complementing radial velocity surveys. Low mass non-transiting objects can currently be detected only if they are isolated (free floating). Orbiting planets are more difficult because of the high star to planet flux ratio. The contrast is smallest in the IR, and hence the most favorable region for planet imaging. Additionally, nulling techniques on interferometers and coronographs can be used to block light from the star. Current developments in adaptive optics suggest direct detection of extrasolar planets may be possible within the next decade.

1.3 Statistical Properties of Observed Systems

The first extrasolar planet, 51 Pegasi b, was reported in 1995 by Mayor & Queloz. It was detected from Haute-Provence Observatory and immediately there after at Keck Observatory by Marcy & Butler (1995). Subsequently, there has been a continuous flux of new systems discovered. The lightest object detected has been 0.0158 M_J.[8] In this statistical analysis, I will only include objects with masses less than 13 M_J, as heavier objects are typically referred to as brown dwarfs. I do not consider planets orbiting pulsars.

1.3.1 Mass

Known extrasolar planets have a wide range of masses, ranging from five Earth masses to over 10 M_J. However, the majority of known extrasolar planets are quite massive.[9] As of now, 37% of the planets detected have masses smaller than 1 M_J and only 13% have masses larger than 5 M_J. Figure 1.1 plots the distribution of known extrasolar planets as of December 2006. A major question facing theoriests has been to explain, as the histogram shows, the significant number of planets ($\sim$ 12%) that have semi-major axes between 0.035 and 0.05 AU ("hot Jupiters").

Additionally, Figure 1.2, plotting semi-major axis versus the projected mass, shows several alarming points. It appears there is a deficit of sub-Jupiter mass planets beyond 0.5 AU, where 57% of the planets are located. The dashed lines in the figure show the detection limits for planets in circular orbits at 3 and 10 $\mathrm{m\,s^{-1}}$, respectively. It is not clear if this deficit is the result of an observational bias (Udry et al. 2003). Also, there are few massive planets ($\geq$ 4 M_J) closer than 0.3 AU to the star. Since observations favor close massive planets, this is not an observational bias, suggesting a minimum distance where gas giants can exist in planetary systems.

1.3.2 Eccentricity

The observed eccentricities of extrasolar planets range over the entire allowed spectrum, but the majority of extrasolar planets have quite high eccentricities (up to 0.93), as shown in Figure 1.3. Over half of the observed extrasolar planets have eccentricities above 0.2, including multi-planet systems housing planets with eccentrities above 0.6. This is in stark contrast to planets in our solar system, which have eccentricities all below 0.1, with the exception of Mercury.[10] For further comparison, the largest eccentricity in the gas planets is Saturn, with $e = 0.054$. The upper limit of 0.93 may be special, as it could be due to secular perturbations of the planet HD 80606 b by a stellar companion on an inclined orbit (Wu & Murray 2003). It also appears that more distant planets tend to

[8] Or equivalently, 5.03 Earth-masses.

[9] This should not suggest that most planets are massive, remember, this is an observational bias. We believe the majority of planets are closer to Earth-size planets.

[10] And Pluto, too.

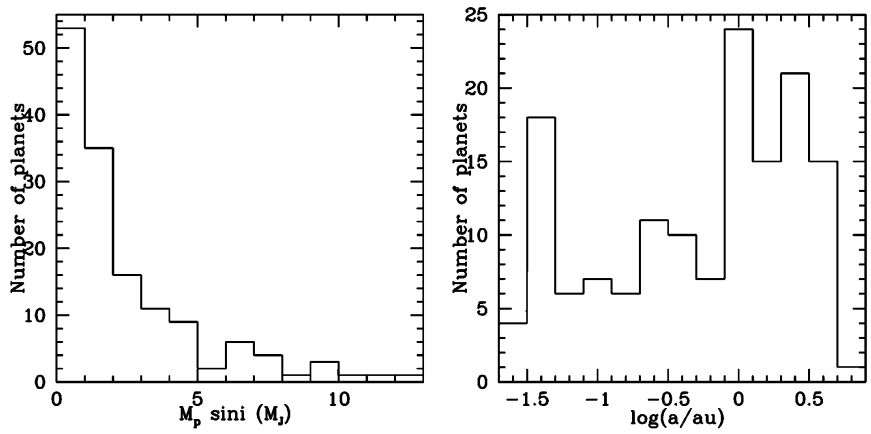

Figure 1.1: Distribution of projected mass $M_p \sin i$ (in M_J, *left panel*) and semi-major axis a (in AU, *right panel*) for known extrasolar planets.

have higher eccentricities. The question to consider is what physical processes occur to create these eccentricities, and does it create either higher eccentricities for larger mass planets or higher eccentricities for larger orbital separations? Artymowicz (1992) suggests disc interactions can create larger eccentricities for larger mass planets, while tidal circularization explains why we observe small eccentricities for short period orbits (Rasio et al. 1996).

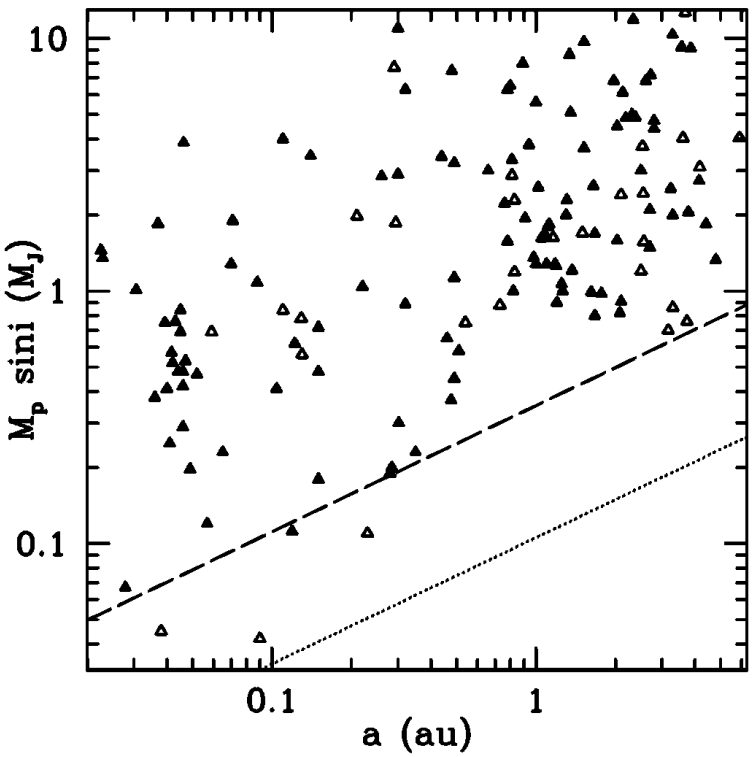

Figure 1.2: Projected mass $M_p \sin i$ (in M_J) vs semi-major axis a (in AU) for known extrasolar planets. Planets in multiple systems are indicated by open symbols. The dotted and dashed lines represent the detection limit for planets on circular orbits and an accuracy of 3 and 10 $\mathrm{m\,s^{-1}}$, respectively.

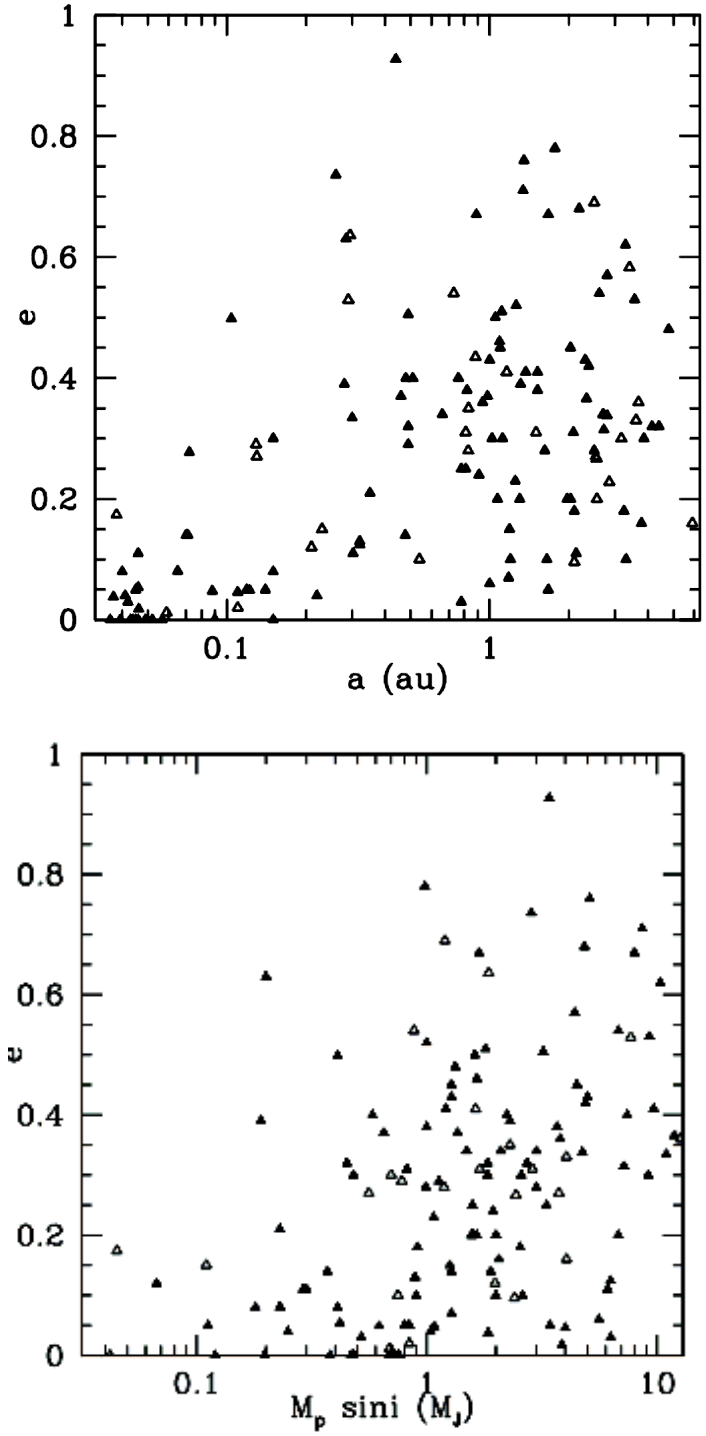

Figure 1.3: Eccentricity vs semi-major axis (in AU, *top panel*) and projected mass $M_p \sin i$ (in M_J, *bottom panel*) for known extrasolar planets. Planets in multiple systems are indicated by open symbols.

Chapter 2

Physical Processes in Discs

In this chapter, I will begin by briefly reviewing the current models of planet formation, focusing on planetesimal and gas giant formation. I then discuss the planet-disc interactions and how this leads to orbital migration and resonance trapping. From there, I will review some of the previous work done on resonance trapping and eccentricity excitation, discussing particular accomplishments and further questions incited from these studies. Finally, I will outline my research.

Protoplanetary discs exist around T Tauri stars, which are a class of pre-main sequence stars named after their prototype T Tauri. They are identified by their optical variability and strong chromospheric lines. Roughly half of T Tauri stars show evidence of a gaseous disc, which is estimated to dissipate on timescales of up to 10^7 yr. Protoplanetary discs around T Tauri stars differ from the discs surrounding close binary systems in their size and temperature. Protoplanetary discs have radii up to 1000 AU and are rather cool. Only the innermost part of the disc reach temperatures above 1000 K.

2.1 Planet Formation

Terrestrial planets are believed to form from solid body accretion of km-sized objects, which are the result of sedimentation and collisional growth of dust grains in protoplanetary discs (see Lissauer 1993 and references therein). This was originally stated in the 19th century from the idea that Earth formed from meteoritic material. Geologist T. C. Chamberlin describes these objects as "planetesimals," sub-Earth to Earth-size solid objects that through collisions can form larger planets. It was not until the 1960's, however, that the theory was developed in detail by V. Safronov (1969). A major accomplishment of this theory was to suggest that gas giants also form in this manner. We will see how large rocky cores can lead to gas giants below.

Terrestrial planets and core formation

Rocky planets and planetary cores form in several stages. First, micron-size dust within the disc forms sediments that settles toward the midplane. This occurs because gravitational interactions with the central body causes the dust in the disc to undergo damped oscillations. The damping occurs because of frictional forces from the gas. Without damping, the dust would oscillate about the rotational plane, by the conservation of angular momentum, at the Keplarian angular velocity

$$\Omega = \sqrt{\frac{GM_*}{r^3}}. \tag{2.1}$$

Additionally, the dust tends to drift toward the star, because its coupling with the gas forces it to rotate at a slightly sub-Keplerian velocity. This means that the dust rotates slightly slower than an object would at a given radius without the presence of a drag force.[1] Assuming the dust particles are spherically shaped with radius r_d, and c_s is the thermal velocity of the gas, the drag force exerted by the gas is $\sim \pi r_d^2 \rho c_s(\mathbf{v_{gas}} - \mathbf{v_d})$, provided that $(\mathbf{v_{gas}} - \mathbf{v_d}) << c_s$ (Epstein law; e.g., Weidenschilling 1977). For a dust grain of mass m_d, we define a characteristic timescale

$$\tau_e = \frac{m_d}{\pi r_d^2 \rho c_s} \tag{2.2}$$

as the time it takes the velocity of the grain to decrease by a factor e. It is from the fact that $2\pi/\Omega >> \tau_e$ that the oscillations are suppressed and the grains sediment toward the midplane. Assuming adopted values of $\rho \sim 10^{-10}$ $\mathrm{g\,cm^{-3}}$, $c_s \sim 10^5$ $\mathrm{cm\,s^{-1}}$, and assuming the density of the grains to be 3 $\mathrm{g\,cm^{-3}}$ (which is comparable to the mass density of the Earth's crust and that of the asteroids) we get $\tau_e \sim 10$ s. For a highly damped harmonic oscillator, this defines a characteristic timescale for sedimentation,

$$\tau_s = \frac{1}{\Omega^2 \tau_e}. \tag{2.3}$$

Using the values above, we can approximate this timescale as $\tau_s \approx 10^5$ yr at 1 AU. This is small compared to planet formation timescales, as we shall see. Collisions and accumulation continues until the objects grow into cm-sized objects. The process of how these objects become km-sized objects is still unclear. Safronov (1969) and Goldreich & Ward (1973) independently pointed out that dust may concentrate in the layers that undergo gravitational instability. These processes would then require the mass density of the dust to be on order of 10^{-7} $\mathrm{g\,cm^{-3}}$. Fragmentation of these layers would then produce km-sized planetesimals. Widenschilling (1980) refuted this theory, however, by showing that, if dust densities were this high, the dust would drag the gas at Keplerian velocities around the star. This would produce a velocity shear between the dust layers and gas around it, giving rise to Kelvin-Helmholtz

[1] Mathematically, its velocity is given by $v = \Omega r - \Delta v$, where $\Delta v > 0$.

instabilities. Dust mixing would result, preventing the densities from getting large enough for gravitational instability to occur.

At this point, further collisions lead to larger planetesimals. It is believed that this process begins with runaway growth and forms a population of small cores. From here, runaway growth ceases and oligarchic growth occurs among these cores. As accretion continues, these cores further isolate themselves, where disc-planet interactions may become important. This process is estimated to take on the order of a few million years.

Gas giant formation

Two theories have been proposed for gas giant formation. The first states that gas giants form through the collapse and fragmentation of the protoplanetary disc. It was first proposed by LaPlace in 1796 and later developed by G. Kuiper in the 1950's (see also, Boss 2006; Boss & Durisen 2005; Mayer et al. 2007). The second theory, proposed by Cameron in 1973, is called the "core accretion model." A solid core is first assembled, as outlined above, until it becomes massive enough to gravitationally bind the surrounding gas it is embedded in. This causes a gaseous envelope to form around the core.

Mizuno (1980) first showed that a gaseous envelope bound to a planetesimal cannot remain in hydrostatic equilibrium if the core exceeds 10-15 M_E. At this time, rapid accretion occurs by the core, converting the rocky core into a gas giant. A gas giant's envelope is acreeted on the order of $\leq 10^5$ yr (Pollack et al. 1996). A problem with this model is that it does not explain what *stops* the accretion. It is possible that the gas is dispersed rapidly during the accretion phase, but timing constraints (dispersal in $\leq 10^5$ yr) make this unlikely. One explanation is that gravitational tides become strong enough to "repel" nearby gas (Lin & Papaloizou 1993).

2.2 Tidal Interactions

The discovery of "hot Jupiters" led to the realization of the importance of orbital migration. Since it is difficult to form a core at small radii, it is proposed that the planet formed at larger radii and migrated inward. Three mechanisms have been developed to explain the locations of planets at very short orbital distances. The first relies on the gravitational interaction between two or more Jupiter mass planets, which may lead to orbit crossing and the ejection of one planet while the other is left in a smaller orbit (Rasio & Ford 1996, Weidenschilling & Marzari 1996). This can account for some but not all of the relatively large number ($\sim 20\%$) of short-period planets observed. A second mechanism is migrational instability (Murray et al. 1998; Malhotra 1993). This involves resonant interactions between the planet and planetesimals located inside its orbit, which lead to the ejection of a fraction while simultaneously causing the planet to migrate inwards. This, however, requires massive discs that would be marginally gravitationally stable. The final mechanism involves tidal inter-

actions between planets and the surronding gas (Goldreich & Tremaine 1979, 1980; Lin & Papaloizou 1979,1993). I will focus on the last of these mechanisms.

Three types of migration have been proposed. These are (1) type I migration, which applies to an embedded protoplanet of small mass where the disc response can be analyzed analytically (e.g., Ward 1997), (2) type II migration, which applies for massive protoplanets that have opened a gap (Lin & Papaloizou 1986), and (3) type III migration, or runaway migration, which is a rapid migration applicable to more massive discs (Masset & Papaloizou 2003; Artzmowicz 2004). Orbital migration occurs through the exchange of angular momentum between the planetesimal and the disc. This can be accounted for by considering viscosity and wave fluxes of angular momentum within the disc, as well as the difference between the rate of advection of angular momentum by gas flowing through the orbit. Additionally, migration can occur due to the rate of increase in the angular momentum content of regions in the neighborhood of the planetesimals due to non steady conditions. The angular momentum carried in waves is associated with type I and type II migration, whereas advected fluxes are associated with type III migration. I will not discuss type III migration here, as most of the theory supporting this process is still in development.

The essential physics of these interactions can be shown by using the impulse approximation (see e.g., Lin & Papaloizou 1979). The gravitational tidal interactions allow angular momentum to be transferred from the gas on the inside to the planet and from the planet to the gas on the outside. Since orbital angular momentum must increase outward in dynamically stable discs (the Rayleigh criterion; Drazin & Reid 1981), gas interior to the planet loses angular momentum and must move farther inward. Similarly, gas outside the planet gains angular momentum and must move farther outward. In effect, the gravitational tides of a planet *repel* the nearby gas. In fluid dynamics, the tides of the planet excite spiral density waves that propagate away from the planet (Goldreich & Tremaine 1979). The waves become excited at the Lindblad resonances, locations in the disc where the natural frequency of radial oscillation is an integer multiple of the frequency at which the gas is forced by the planet. That is,

$$\pm m(\Omega(r) - \Omega_p) = \Omega(r), \tag{2.4}$$

where Ω_p is the orbital frequency of the planet, $\Omega(r)$ is the orbiting frequency of the gas at radius r, and m is a positive integer. The torque exerted on the gas is the sum of the contributions from the Lindblad resonances and is negative (positive) for gas interior (exterior) to the planet. The expression for the torque is given by (Lin & Papaloizou 1993)

$$T_{tide} = f\Sigma\Omega_p^2 r_p^4 \left(\frac{r_p}{H}\right)^3 \left(\frac{M_p}{M_*}\right)^2, \tag{2.5}$$

where H is the height of the disc, Σ is the surface density, and $f \approx 0.2$ is a constant. This torque tends to push gas away from the planet, whereas the viscous stress of the gas seeks to diffuse gas back toward the planet and is given

by (Lynden-Bell & Pringer 1974)

$$T_{vis} = 3\pi\Sigma\nu\Omega r^2 = 3\pi\alpha\Sigma\Omega^2 r^4 \left(\frac{H}{r}\right)^2, \tag{2.6}$$

where α is a dimensionless parameter and ν is the viscosity. Therefore, we would expect that a gap forms when $T_{tide} \geq T_{vis}$. We then arrive at the expression for the minimum mass required to open a gap:

$$\frac{M_p}{M_*} \geq \sqrt{\alpha}\sqrt{\frac{3\pi}{f}} \left(\frac{H}{r}\right)^{5/2}. \tag{2.7}$$

Using typical values adopted for discs, this gives us a mass $\sim 75 M_E$, slightly less than the mass of Saturn. It is also possible that these gap-forming processes serve as a way to terminate the gas accretion on the solid cores.

However, for planets smaller than this gap-forming limit, the exchange of angular momentum between the gaseous disc and the planet can result in orbital migration. The angular momentum of the planet is given by

$$M_p \Omega_p r_p^2 = M_p \sqrt{G M_* r_p}, \tag{2.8}$$

and therefore the *net* total torque exerted by the planet on the gas, T_{net} is governed by

$$\frac{d}{dt}\left(m_p \Omega_p r_p^2\right) = -T_{net}, \tag{2.9}$$

or equivalently,

$$\frac{dr_p}{dt} = -\frac{T_{net}}{2 m_p \Omega_p r_p}. \tag{2.10}$$

This defines a characteristic timescale for type I migration

$$t_{migI} = \frac{r_p}{|dr_p/dt|} = \frac{\Omega_p r_p^2}{2T_{net}} \sim \frac{1}{\Omega_p}\frac{M_*}{M_p}\frac{M_*}{\Sigma r_p^2}\left(\frac{H}{r}\right)^2, \tag{2.11}$$

where I estimated T_{net} as T_{tide} reduced by H/r (Ward 1986). Again, this only applies to smaller planets that cannot form gaps; more massive planets within gaps have surface densities that drop of significantly. This timescale is surprisingly short, on the order of 10^5 yr for Earth-sized planets. The expected lifetime of these discs are on order of 10^7 yr, which raises the question of why all planets do not eventually migrate into the star? There must be some mechanism that is stopping this runaway migration. I will explore a possible solution in this thesis.

When gap conditions are satisfied, the outward flux of angular momentum due to viscous transport in the outer disc is supplied by the planet, and the angular momentum of the inner disc is taken up by the planet. When the contributions do not balance, the planet's change in angular momentum forces it to migrate. Simulations have indicated that the outward flux dominates,

causing inward migration. This migration also occurs on the viscous timescale and is given by (Shakura and Sunyaev 1973)

$$t_{migII} = \frac{1}{3\alpha}\left(\frac{r_p}{H}\right)^2 \Omega^{-1} = \frac{0.05}{\alpha}\left(\frac{r_p}{H}\right)^2 \left(\frac{r_p}{1\ \mathrm{AU}}\right)^{3/2}. \tag{2.12}$$

We arrive at values on order of $10^3 - 10^4$ yr for r_p between 1 and 5 AU. This is even shorter than estimated planetary formation timescales, let alone the disc lifetime.

Suggestions on how to stop this rapid migration have been proposed. Tidal interactions with the star at small radii would allow for gap-formed planets to cease migration (Lin et al. 2000). Additionally, planets close enough to the star would lose part of their outer envelope as they are accreted onto the star, and this transfer of mass would move the planets outward, allowing for migration to cease (Trilling et al. 1998). Finally, magnetic activity within the gas could also cease migration at small radii. Magnetic activity and tidal interactions with the star account for the location of 51 Pegasi b (Lin et al. 1996), and help to explain the location of hot Jupiters in general. However, these mechanisms cannot account for the presence of gas giants orbiting at distances larger than a tenth of an AU. What is causing these planets to stop migrating? Disc dissipation may account for ceasing the migration. If there was not enough material left in the disc after planet formation occurred, then significant migration could not take place. It has been proposed that several gas giants form in a typical disc and only a handful survive (Lin 1997).

A Possible Solution: Resonance

Orbital migration occurs at different rates within the disc, which depend on the disc parameters, and can produce convergent migration and locking into mean motion resonances–similar to the induced migrations of satellites in the Solar System (Goldreich 1965). When the orbital periods of objects becomes simple ratios, the periodicity of their motion can cause the objects to move as a coupled system. Resonance trapping occurs when the gain of energy and angular momentum of a particle due to resonant gravitational perturbations from a planet exactly compensates for the loss of energy and angular momentum due to an external dissipation, such as gas drag. Pairs of extrasolar planets have been found in such resonance configurations. Gliese 876 (Marcy et al. 2001) and HD 82943 (Mayor et al. 2004) have planets that are in 2:1 resonances, for example. The origins of these commensurable orbits are naturally explained by disc interactions. It has been shown that when a planet migrate inward and lock into resonance with an inner planet, their migration rates are appreciably slowed.

2.3 Review of Previous Work

Resonance Trapping

Much work has been done in trying to determine the importance of resonances in planetary systems and how it relates to (1) the formation and (2) the stability of the systems. We review some of those results here while discussing some of the questions that have arisen from these studies.

Lee (2004) has shown the diversity of the various 2:1 resonance configurations that can be reached in planetary systems by means of migration. The 2:1 resonance can have three possible configurations: (1) Symmetric, where the resonance variables[2]

$$\begin{aligned} \theta_i &= \lambda_i - 2\lambda_o + \varpi_i \\ \theta_o &= \lambda_i - 2\lambda_o + \varpi_o, \end{aligned} \tag{2.13}$$

both liberate about 0°; (2) Anti-symmetric configuration, where θ_i and θ_o liberate about 0° and 180°, respectively, and; (3) Asymmetric configurations, where θ_i and θ_o liberate about angles far from either 0° or 180°.[3] In doing so, he concluded that the mass ratio of the two bodies, m_1/m_2, can strongly affect the possible outcome of the resonance trapping. In particular, some mass ratios are unstable, in that any additional migration would break the resonance, and the planets would move as an uncoupled system once again. Additionally, the magnitude of the eccentricity damping in the migration greatly determines the final outcome of the system, suggesting that even the model of our migration term is important. This frictional term is typically written as

$$f = -\alpha \mathbf{v} + \sum_i g_i(\mathbf{r}, \mathbf{v}), \tag{2.14}$$

where understanding the form of g is one question we must seek to answer. Also, Lee shows that the mass ratio of the bodies plays a substantial role in whether the resonance trapping is stable or not. It would then be useful to understand the role the mass ratio plays in various resonances, so to better understand which resonances have a higher probability of capture under various conditions.

Resonance has been shown to be a crucial factor in determining the outcome of planetary systems. It has been shown that when planets become trapped in mean motion resonance, further migration leads to eccentricity growth. Resonance then serves as a mechanism to create the observed eccentricities in planetary systems.

As mentioned above, GJ 876 contains two planets in a 2:1 resonance. Lee and Peale (2002) have modeled this system by allowing the outer planet to

[2]These can be easily determined from the disturbing function of the N-body system. See, e.g., Murray and Dermott's *Solar System Dynamics*, chapters 6 and 8.

[3]Here λ is the mean longitude, and ϖ is the longitude of pericenter.

migrate and become locked into a 2:1 resonance with the inner planet.[4] In an attempt to recreate the observed properties of the system, Lee and Peale test whether resonance can create the observed eccentricities of the planets, which are 0.27 and 0.1 for the inner and outer planets, respectively. Their first tests use only standard friction to model the migration, without eccentricity damping, and were unable to recreate the observed system.[5] However, they were able to get reasonably close by including an eccentricity damping term into their migration models. However, it required such strong damping that their values did not make sense with existing disc parameter estimates. They suggest that the migration in this system must have been finely tuned to stop when the system had progressed to its observed state, either through disc dissipation or by some other mechanism. It does show that resonance can play a strong role in pumping up eccentricities, and further knowledge of the disc parameters would allow us to determine the maximum eccentricities that could be created.

Eccentricity Excitation

Several mechanisms have been proposed to explain the high eccentricities observed in extrasolar planetary systems. I will outline the three most prominent here.

Gravitational Perturbation by a Companion Star - Most stars are part of binary star systems. This theory suggests that planets orbiting one star can be gravitationally perturbed by the companion star, exciting large eccentricities in the planetary orbits on very long timescales (10^8 yr). This theory is one of the more appealing in general because only a handful of stars known at present to harbor planetary systems also have stellar companions (Schneider 2005).

Interactions with the Protoplanetary Disc - Planets having initial eccentricities exceeding ~ 0.01 (Goldreich & Sari 2002) can have their eccentricity excited due to Lindblad resonances in the protoplanetary disc, in spite of damping from the corotation resonances. Additionally, when migration results with trapping into mean motion resonance, this leads to eccentricity pumping, also in spite of damping forces. It has also been shown that divergent migration (when the planets move away from each other) *through* mean motion resonances can lead to eccentricity excitation (Chiang, Fischer, & Thommes 2002).

Planet-Planet Scattering - Close encounters among planets in the system can lead to large impulsive forces that result in a scattering event where one object may be ejected from the system (Rasio & Ford 1996; Weidenschilling & Marzari 1996). These sudden perturbations have been shown to impart finite eccentricities on the surviving planets (Malhotra 2002),

[4] The projected masses of inner and outer planets are 1.89 M_J and 0.56 M_J, respectively.
[5] I will derive what I mean by eccentricity damping in Section 3.4.

and is a mechanism for scattering planets into higher-order resonances (e.g., 4:1).

2.4 Outline of Thesis

These studies show the substantial role resonances play in the stability and formation of planetary systems. Additionally, various parameters of the system, such as the mass ratio of the two planets, properties of the disc, or the presence of eccentricity damping can greatly alter the final configurations of the system.

The first part of this project is the systematic study of the processes that lead to the formation of planetary systems within a protoplanetary disc. In particular, I focus on the resonance phenomena and the implications of resonant trapping for the evolution of the system. It has been shown that migrating objects can be captured into resonances (Lee & Peale 2002; Kley 2003). These resonances are then locations of high densities of mass, where mass accretion can occur, leading to the formation of planets. The probability of capture depends on a variety of factors. It has been shown, for example, that as giant planets accrete their gaseous envelopes within the disc, this accretion can lead to migration and ultimately instability (Lissauer 1993, 1995). Moreover, the probability is simultaneously affected by the eccentricity, dissipation (migration rate), orbital inclination, and mass ratio between the two objects. I have systemically studied regions of this parameter space in order to determine what factors contribute significantly to the success of resonance captures in conditions similar to those found in real protoplanetary discs. This greatly extends all previous, simplified studies exploring this parameter space (e.g., Quillen 2006).

The dynamical evolution of the system is influenced by the interaction of the planets with the residual gas in the disc. I take into account interactions with a gaseous disc in my simulations. I consider only three-body systems, which will be simulated by orbital dynamical integrations using my code *ResCap*. This code has been fine-tuned over the past year and has been successful in reproducing results consistent with John Chamber's similar software package *Mercury* (Chambers 1999). The migration is controlled through a damping term that is applied to the migrating outer planet. This damping term is set to model the frictional effects of a protoplanetary disc given several parameters, such as the density of the gas and masses of the planets (Thommes 2005). *ResCap* allows for calculations of a wide range of initial conditions throughout this parameter space, allowing me to treat each parameter individually in order to determine its effects, without having to perform full hydrodynamic calculations of the disc.

I find that particular resonances are more stable than others, showing that more planetestimals will collect at certain locations. The results of my research on ideal two-planet, non-eccentric systems have shown that the number of possible mass ratios decreases as the resonance increases in complexity (e.g., 5:4 compared to 2:1). Further study will allow me to obtain the previously unknown mass ratio interval to guarantee capture for initially non-eccentric orbits. Full studies of this parameter space can then follow by slowly increasing eccentricity

and inclination up to critical values that would prevent capture or stability. This process can then be repeated for varying rates of migration. Once the adiabatic limit is crossed, the probability of capture decreases significantly. This study will require significant time in both computation and analysis.

The second part of this project is to study both how dynamical instability can affect the longterm evolution of the system and how it can explain the large number of highly eccentric planets. The gravitational interactions between planets can cause systems to go unstable through either collisions or the ejection of planets (e.g., Rasio & Ford 1996, 2007). In some cases, however, these perturbations can toss planets into highly eccentric orbits. Additionally, gas giants can be thrown into very close orbits around their central star. I place three-body systems in a particular resonance under conditions that will cause the system to become unstable (either through making one of the planets sufficiently massive, having planets with large eccentricities, or using resonances where the orbital separation is small). I find that the probability for dynamic instability depends on the resonance selected and is highly sensitive to the eccentricity of the planets. Highly eccentric orbits have a greater tendency for dynamic instability over circular orbits. Additionally, this mechanism serves as a way to create planets in higher-order resonances (e.g., 4:1 or 5:3) by having planets *tossed* into these resonances.

My research provides the first complete study of the resonance capture phenomena in protoplanetary discs. The results will lead to an improved understanding of an important process involved in the formation and dynamical evolution of extrasolar planetary systems. In doing so, we will gain a stronger understanding of our own solar system's origins as well as qualify the existence of habitable systems outside our own.

Chapter 3

Numerical Setup: *ResCap*

ResCap is a fourth-order Runge-Kutta N-body integrator that I developed over the summer of 2006. I include the entire code, which is written in C, as Appendix B. The code allows for the integration of planetary systems over arbitrarily long timescales, similar to leading software packages such as Chamber's *Mercury* (Chambers 1999). I have chosen to have *ResCap* integrate Newton's laws of motion rather than Hamilton's equations. Integrators that integrate the latter are referred to as symplectic integrators. My N-body integrator easily allows for external parameters, such as friction, to be incorporated for individual planets. However, symplectic integrators are known to have two important advantages over other algorithms. First, they exhibit no long-term build up in energy error. Second, the motion of each object about the central body can be "built in," so that the choice of timestep is determined by the perturbations between bodies, whose magnitude can be substantially smaller than the forces due to the central body (Wisdom & Holman 1991). These two factors will have to checked in order to ensure *ResCap* can work properly. We will first review the basic structure of Runge-Kutta integrators, and then the structure of *ResCap* in detail.

3.1 Runge-Kutta Method

Problems involving ordinary differential equations (ODEs) can always be recasted as a set of first-order differential equations. For example, the equation

$$\frac{d^2y}{dx^2} + h(x)\frac{dy}{dx} = g(x) \tag{3.1}$$

can be rewritten as the set of differential equations

$$\begin{aligned} \frac{dy}{dx} &= z(x) \\ \frac{dz}{dx} &= g(x) - h(x)z(x) \end{aligned} \tag{3.2}$$

$$, \tag{3.3}$$

where z is introduced as a new variable to signify the derivative of the original variable y. It could also be useful to incorporate into these variables additional factors, such as powers of the independent variable (e.g. let $z = x^2 y$), so to mitigate singular behavior that could result in overflows or roundoff errors.

The original problem then reduces to solving a set of first-order differential equations. This, along with a set of initial conditions, allows us to numerically solve the equations of motion. The underlying idea of solving the linear first-order initial value problem is the rewrite the dy's and dx's as finite steps Δy and Δx, and multiply Equation 3.3 by Δx. In the limit of Δx being very small, a good approximation can be achieved. Literal use of this method is referred to as *Euler's Method*, but is not recommended for practical use. However, the concept *is* important; all methods typically come down to the same idea. The Runge-Kutta method propagates a solution over an interval by combining the information from several Euler-style steps (each involving one evaluation of the right-hand side of Equation 3.3) and then using the information obtained to match a Taylor series expansion up to some higher order. Another popular method is the Bulirsch-Stoer method. It is a powerful idea of extrapolating a computed result to the value that *would* have been obtained if the stepsize had been much smaller that it actually was. It gains an advantage over Runge-Kutta in efficiency, but works better for "smooth" problems, that is, problems that would not require the timestep to be increasingly small. Runge-Kutta succeeds virtually always; but it is not usually the fastest. However, the timescales required for my simulations ($\leq 10^7$ yr) makes Runge-Kutta an ideal choice.

3.1.1 Derivation of the Method

The formula for the Euler method is

$$y_{n+1} = y_n + hf(x_n, y_n) + O(h^2)^1 \tag{3.4}$$

which advances the solution from x_n to $x_{n+1} = x_n + h$. This formula is unsymmetrical in that it advances through an interval h but uses derivative information only from the beginning of the interval. Additionally, the Taylor expansion in Equation 3.4 shows that the error is only one order of h smaller than the correction, making this a *first-order* approximation. Using this method directly is (1) not very accurate compared to other algorithms, and (2) unstable for complex sets of equations. Consider, however, the use of a "trial step," to the midpoint of the interval. Then use the values of both x and y at the midpoint to reevaluate the derivatives and use those values to get to the real values across the whole

[1] Where higher orders of h have been supressed. These terms originated by simply taking a power series of Δy about h.

interval. That is, use the following set of equations to evaluate y_{n+1}

$$\begin{aligned} k_1 &= hf(x_n, y_n) \\ k_2 &= hf(x_n + \tfrac{1}{2}h, y_n + \tfrac{1}{2}k_1) \\ y_{n+1} &= y_n + k_2 + O(h^3). \end{aligned} \tag{3.5}$$

The symmetry cancels out the first-order errors, making this a *second-order* method, and is typically referred to as the *second-order Runge-Kutta method*. This is still not ideal for practical use (when small errors are necessary over long timescales). However, the second-order method encapsulates the basic idea of Runge-Kutta: by taking the right combination of trial steps, we can cancel out higher order error terms.

The *fourth-order Runge-Kutta method* is what we will be interested in. It gives fourth-order accuracy without significant computational time. In doing so, we will compute two midpoints, and use them to project towards the final point. The equations for the fourth-order Runge-Kutta method are:

$$\begin{aligned} k_1 &= hf(x_n, y_n) \\ k_2 &= hf(x_n + \tfrac{1}{2}h, y_n + \tfrac{1}{2}k_1) \\ k_3 &= hf(x_n + \tfrac{1}{2}h, y_n + \tfrac{1}{2}k_2) \\ k_4 &= hf(x_n + h, y_n + h) \\ y_{n+1} &= y_n + \tfrac{k_1}{6} + \tfrac{k_2}{3} + \tfrac{k_3}{3} + \tfrac{k_4}{6} + O(h^5). \end{aligned} \tag{3.6}$$

This method requires four evaluations of the right-side equations of Equation 3.3, once at the initial point, twice at trial midpoints, and once at a trial endpoint. Combined with some additional features I will describe below, this method can be very powerful. However, if *very* high accuracy is required, we will see that computation time can become an issue for Runge-Kutta. We will compare computational time versus accuracy in Section 3.3.

3.1.2 Adaptive Stepsize

At the beginning of the integration, a stepsize (our h) must be specified. It does not make sense that this stepsize should remain constant throughout the entire integration. We should require smaller stepsizes when integrating through, for example, a close encounter, where the planets' gravitational effects dominate their motion, compared to when they are orbiting their central star stably. However, having a small stepsize throughout the entire integration is overkill, because we will lose significant time waiting for the integration to compute up to and after the close encounter, where nothing interesting would be going on. Likewise, if our stepsize is too large, we could model our close encounter incorrectly (and even result in events like collisions, which may not have occurred had we had a smaller stepsize, giving us incorrect results). Therefore, I implement an adaptive stepsize in *ResCap*, allowing it, if I may use an analogy, to move slowly through treacherous terrain, while speeding through smooth uninteresting countryside. While doing this, I can still maintain a predetermined order of

accuracy, which is continuously monitored at every step. Obviously, this leads to additional computations per timestep, but the gain we will receive will be well worth it.

The basic idea is that of *step doubling*. That is, we take each step twice, once as a full step (to arrive at $y_{n+1,1}$), then once as two half steps (which is naturally more accurate) to arrive at $y_{n+1,2}$. We then compare the difference of the two equations,

$$\Delta = y_{n+1,2} - y_{n+1,1}, \tag{3.7}$$

which we label as the *truncation error*. It is in Δ that we can measure our accuracy, and adjust h accordingly. I will use a method developed by Fehlberg (1969), which is based off this idea. He realized that Runge-Kutta methods of order M (M $\geq$ 4) require between M and M+2 function evaluations total. For example, in a crude step doubling algorithm, the initial point for both the full step and half steps is the same, and would only need to be computed once. Fehlberg discovered a fifth-order method with six functions evaluations where another combination of the six functions gives a fourth-order method. The difference between the two estimates of y_{n+1} can be used, similar to our step doubling method, to determine the truncation error.

The general form of a sixth-order Runge-Kutta formula is the following set of equations:

$$\begin{aligned} k_1 &= hf(x_n, y_n) \\ k_2 &= hf(x_n + a_2 h, y_n + b_{21} k_1) \\ &\vdots \\ k_6 &= hf(x_n + a_6 h, y_n + b_{61} k_1 + \cdots + b_{65} k_5) \\ y_{n+1} &= y_n + c_1 k_1 + \cdots + c_6 k_6 + O(h^6). \end{aligned} \tag{3.8}$$

The embedded fourth-order formula is

$$y^*_{n+1} = y_n + c^*_1 k_1 + \cdots + c^*_6 k_6 + O(h^5), \tag{3.9}$$

so that the truncation error is given as

$$\Delta = y_{n+1} - y^*_{n+1} = \sum_{i=1}^{6} (c_i - c^*_i) k_i. \tag{3.10}$$

The values of c_i, b_{ij}, and a_i have been calculated by Cash and Karp (1990) and are given in the following table.

Now how does Δ relate to h? According to Equations 3.8 and 3.9, Δ scales as h^5. If we take step h_1 to produce an error Δ_1, then a step h_0 would have given some other value Δ_0, which is easily estimated as

$$h_0 = h_1 \left| \frac{\Delta_0}{\Delta_1} \right|^{1/5}. \tag{3.11}$$

Let us define Δ_0 as our *desired error*–determined at the start of the integration. This equation is then used in three ways:

Cash-Karp Parameters for Runge-Kutta								
i	a_i	b_{ij}					c_i	c_i^*
1							$\frac{37}{378}$	$\frac{2825}{27648}$
2	$\frac{1}{5}$	$\frac{1}{5}$					0	0
3	$\frac{3}{10}$	$\frac{3}{40}$	$\frac{9}{40}$				$\frac{250}{621}$	$\frac{18575}{48384}$
4	$\frac{3}{5}$	$\frac{3}{10}$	$\frac{-9}{10}$	$\frac{6}{5}$			$\frac{125}{594}$	$\frac{13525}{55296}$
5	1	$\frac{-11}{54}$	$\frac{5}{2}$	$\frac{-70}{27}$	$\frac{35}{27}$		0	$\frac{277}{14336}$
6	$\frac{7}{8}$	$\frac{1631}{55296}$	$\frac{175}{512}$	$\frac{575}{13824}$	$\frac{44275}{110592}$	$\frac{253}{4096}$	$\frac{412}{1771}$	$\frac{1}{4}$
$j =$		1	2	3	4	5		

- If $\Delta_1 > \Delta_0$, we must *decrease* the stepsize and retry the present (failed) step.
- If $\Delta_1 < \Delta_0$, this equation tells us how much we can safely *increase* the stepsize for the next step.
- If $\Delta_1 = \Delta_0$, then our stepsize is working perfectly and no adjustment is needed for the next step.

This algorithm allows *ResCap* to work slowly through complex regions while sailing through easier regions of the integration.

3.2 Set-Up

ResCap is used to model resonance trapping in N-body systems. However, all derivations and results from this point forward will be for three-body systems, but it will be clear how the procedure can be easily generalized. The type of resonance trapping I will be considering in these three-body systems is by having the outer body migrate inward and getting captured into resonance with an inner body. The procedure to control this migration will be described in Section 3.4.

Before determining the initial conditions of the bodies, it is important to understand what the parameters of *ResCap* are. It seems natural to begin by defining our units.

3.2.1 Units

It is natural to non-dimensionalize our units when dealing with orbiting bodies. Therefore, we need to convert from metric units (kg, m, s) to a new unit system $(\tilde{M}, \tilde{L}, \tilde{T})$ by some map ϕ. We do so by the following prescription.

- Scale the masses by the mass of the central star, M_*. That is, define

$$\tilde{M} = M_* \equiv 1.$$

Then the masses of the inner and outer body become $\tilde{M}_i = M_i/M_*$ and $\tilde{M}_o = M_o/M_*$, respectively.

- In the integrations, a particular resonance is typically expected. Therefore, the two planets will be set up so, after some migration takes place, the outer body will pass the location where resonance trapping can occur, i.e., where the ratio of the planets' periods will give the desired ratio.[2] This radii, r_{res}, measured from the origin, is then what we will scale our distances to, that is,
$$\tilde{L} = r_{res} \equiv 1.$$
Therefore, the coordinates of the three bodies are given as $\{\tilde{x_j}, \tilde{y_j}\} = \{x_j/r_{res}, y_j/r_{res}\}$, where $j \in \{*, i, o\}$.

- Set the gravitational constant to unity,
$$G \equiv 1.$$
Out unit of time is determined by these three scalings. Rearranging Kepler's third law (Eqn 1.3), omitting the $4\pi^2$, we have
$$T = \frac{a^{3/2}}{\sqrt{GM_*}}, \tag{3.12}$$
which has units of seconds and is written in terms of our three parameters we wish to rescale. Therefore, in our new units, we define our "unit" of time as
$$\tilde{T} = \frac{r_{res}^{3/2}}{\sqrt{GM_*}}. \tag{3.13}$$
In the majority of these simulations, r_{res} will be 1 AU, and M_* will be a solar mass. Substituting into the above equation, we get that
$$\tilde{T} = 6.0231 \cdot 10^6 \text{ sec.}$$
Therefore, we rescale the original time t by $\tilde{T}$. From now on, when I refer to a "timestep," I am referring to 1 $\tilde{T}$.

These three conversions define our map $(kg, m, s) \xrightarrow{\phi} (M_*, r_{res}, \tilde{T})$ to non-dimensional units. It is common to refer to the non-dimensional units with an overhead tilda, e.g. $\tilde{x}$.

3.2.2 Frame of Reference: Initial Conditions

The initial conditions of the three bodies depends on the frame of reference. For *ResCap*, I have selected the center of mass frame of reference, that is, the

[2] We will see how this is determined in the next subsection.

center of mass is at the origin. The initial conditions are then determined in the following way.[3]

As mentioned above, each simulation is set up with a particular resonance in mind. This provides us with an additional constraint that will help determine the initial conditions. Resonances are typically written of the form

$$\frac{p}{p+q}$$

where p and q are nonnegative integers. For example, a 2:1 resonance would have $p = q = 1$. Resonance gives a relation between the orbital periods, which then gives a relation between the semi-major axes using Kepler's third law, that is if

$$\frac{T_i}{T_o} = \frac{p}{p+q} \equiv \Re, \tag{3.14}$$

then we have that

$$\frac{a_i^{3/2}}{a_o^{3/2}} = \Re. \tag{3.15}$$

This gives the following relation:

$$a_i = \Re^{2/3} \cdot a_o. \tag{3.16}$$

regardless of our choice of units. Now we originally said we were going to scale the distance so the location of this resonance is for the outer planet is 1. So the above equation immediately gives us the initial semi-major axis of the inner planet as simply $\tilde{a}_i = \Re^{2/3}$. The mean motion velocity can then be determined by using the relation $\tilde{n} = 2\pi/\tilde{T}$,

$$\tilde{n}_i = \frac{2\pi}{\tilde{T}_i} = 2\pi \frac{\sqrt{\tilde{M}_* + \tilde{M}_i}}{2\pi\ \tilde{a}^{3/2}} = \frac{\sqrt{1 + \tilde{M}_o}}{\Re}. \tag{3.17}$$

Here, I have returned to using the original form of Kepler's third law, where the sum of the masses is not approximated as the central mass.[4] Before I deduce the initial conditions of the inner planet, I must introduce two more parameters. It may be desirable to place the planets outside the resonance locations by making small adjustments to their position coordinates. For example, I will typically place the outer planet slightly out of the resonance location by making this small adjustment. This can be done manually by adding a "shift" term to the initial position coordinates. I then state that the initial position (with the central body at the origin) of the inner planet is

$$\begin{aligned} \tilde{x}_i &= \Re^{2/3} + \tilde{x}_{i,adjust}, \\ \tilde{y}_i &= 0 + \tilde{y}_{i,adjust}. \end{aligned} \tag{3.18}$$

[3]For a derivation of all the formulae used in this section, consult Murray and Dermott's *Solar System Dynamics*, Ch. 2.

[4]This is a personal preference, we could have continued to use the approximated version without harm as long as the planets' masses are small relative to the central object.

I have selected the inner planet to lie on the x-axis (This is arbitrary for two-bodies, given any other initial position, a simple rotation could place the planet on the x-axis).

For the outer body, the initial position is similarly determined, but another parameter needs to be introduced. While the location of two bodies is rotationally invariant, this is not true for three bodies. The third body could be anywhere on its orbit relative to the inner planet.[5] Typically, this parameter is randomized between 0 and 2π, and determines the location on the orbit relative to the inner planet. Here, we are measuring the angle, ϕ, relative to the positive x-axis. Then the initial position of the outer planet is given by

$$\begin{aligned} \tilde{x}_o &= \frac{(1+\tilde{x}_{o,adjust})(1-e_o^2)}{1+e_o\cos\phi}\cdot\cos\phi, \\ \tilde{y}_o &= \frac{(1+\tilde{y}_{o,adjust})(1-e_o^2)}{1+e_o\cos\phi}\cdot\sin\phi, \end{aligned} \tag{3.19}$$

where e_o is the desired initial eccentricity of the outer planet.[6] It is not hard to see that this is nothing more than the polar parameterization of an ellipse projected onto the x and y-axis. We have now calculated the initial positions of the system with the central object at the origin.

We now can calculate the center of mass of the system. Since we are setting the center of mass to be located at the origin, we can readily solve the equations

$$\frac{\tilde{M}_*\tilde{x}_* + \tilde{M}_i\tilde{x}_i + \tilde{M}_o\tilde{x}_o}{\tilde{M}_* + \tilde{M}_i + \tilde{M}_o} = 0, \tag{3.20}$$

and similarly for y, to determine the initial position of the star in the center of mass frame,

$$x_* = -\frac{\tilde{M}_o\tilde{x}_o + \tilde{M}_i\tilde{x}_i}{\tilde{M}_*}. \tag{3.21}$$

However, Equations 3.18-3.19 assume the star is at the origin, so we append $\tilde{x}_*$ and $\tilde{y}_*$ to the initial positions of the planets, to maintain the correct relative distance. For example,

$$\tilde{x}_i = \Re^{2/3} + \tilde{x}_{i,adjust} \rightarrow \tilde{x}_i = \Re^{2/3} + \tilde{x}_{i,adjust} + \tilde{x}_*. \tag{3.22}$$

We can now calculate the initial velocities of the three objects. For the inner planet, its initial velocity is given as

$$\begin{aligned} \tilde{v}_{i,x} &= 0 \\ \tilde{v}_{i,y} &= \frac{\tilde{n}_i\tilde{a}_i}{\sqrt{1-e_i^2}}(1+e_i) \\ &= \frac{1+e_i}{\sqrt{1-e_i^2}}\cdot\sqrt{\frac{\tilde{M}_* + \tilde{M}_i}{\tilde{x}_o}}, \end{aligned} \tag{3.23}$$

[5] Unless for the particular simulation we are beginning the simulation with the planets in resonance, which then we may wish to start the two planets both along the x-axis.

[6] If we wanted to give the inner planet an initial eccentricity, we could arrive at a similar equation.

and similarly for the outer planet,

$$\begin{aligned}\tilde{v}_{o,x} &= -\frac{\tilde{n}_o\tilde{a}_o}{\sqrt{1-e_o^2}}\sin\phi \\ \tilde{v}_{o,y} &= \frac{\tilde{n}_o\tilde{a}_o}{\sqrt{1-e_o^2}}(\cos\phi + e_o).\end{aligned} \tag{3.24}$$

From this, we can use the fact that we want to center of mass to remain stationary at the origin to determine the initial velocity of the star. That is, we solve the equations

$$\tilde{M}_*\tilde{v}_{*,j} + \tilde{M}_i\tilde{v}_{i,j} + \tilde{M}_o\tilde{v}_{o,j} = 0, \tag{3.25}$$

where $j \in \{x, y\}$. We have determined the initial conditions of the system. By inputing the initial masses, eccentricities, and any additional adjustments in the position of the bodies, the initial conditions can be determined.

3.2.3 The Equations of Motion

This initial value problem requires 12 initial conditions, two position coordinates and two velocity coordinates per body. Therefore, we need 12 differential equations. Six of these will be trivial, and the remaining six will simply be Newton's law: six equations to describe the change in position, and six to describe the change in velocity. They can be summarized as the following, regardless of choice of units:

$$\begin{aligned}\frac{dx_j}{dt} &= v_j, \\ \frac{dv_{j,x}}{dt} &= \frac{M_{j+1}}{r_{j,j+1}^3}(x_{j+1}-x_j) + \frac{M_{j+2}}{r_{j,j+2}^3}(x_{j+2}-x_j) + f_x^j,\end{aligned} \tag{3.26}$$

where $j \in \{*, i, o\}$, and $\{j, j+1, j+2\}$ is a cyclic permutation of elements of the set $\{*, i, o\}$. The $r_{j,j+1}$ factor is the vector magnitude of the relative distance between the j and $j+1$ bodies. Similarly for $r_{j,j+2}$. The term f_x^j is an additional term where migration will be incorporated for the j-th body in the x-direction, else it is set to zero. The form of this term will be derived in Section 3.4. There is an identical set of equations for the y-direction.

Additionally, some integrations will ask for mass accretion, that is, to allow the mass of the bodies to change over time. We then include three additional equations

$$\frac{dM_j}{dt} = f(x_j, y_j, \alpha) \tag{3.27}$$

where f is a function that can depend on the location of the body plus any additional parameters, α. The simulations that will use these equations will allow the mass to grow linearly, so that f is a constant.

3.2.4 Additional Parameters of *ResCap*

There are several additional parameters that need to be determined prior to integrations. These, however, do not need to be adjusted for every simulation.

Error Control

Three parameters must be determined for the error control program, outlined above. The value of Δ_0, the allowed error per timestep, must be stated. Additionally, the initial value of h must be given, h_0, which I will take to always be equal to 10^{-14}. Therefore, the error control program can slowly increase h if $\Delta_1 < \Delta_0$ in Equation 3.11, but it is small enough so that if the program starts in a complicated regime, it is ready to use small timesteps. Finally, the minimum allowed timestep h_{min} must be given, which I will take to be 0. If one wished to be cautious and avoid possible underflows, one may want to set this to 10^{-30}. We will determine what value of Δ_0 to use in Section 3.3.

Printing Data: The Flow of *ResCap*

The length of the integration is determined as follows. Rather than running one long integration, *ResCap* runs multiple smaller runs in succession. For example, *ResCap* will solve the equations of motion for $T = 0$ to $T = 1000$ yr. From there, it prints the data from that integration. It will then clear its memory and input the final conditions of the previous run as the initial conditions of the next run, and use that to integrate from $T = 1000$ to $T = 2000$ yr, continuing until the integration is complete.

As the reader, you may wonder how my error program handles this, because no matter what h happened to be at the end of run, it will be reset to h_0 at the start of the next integration. This is the reason I have chosen h_0 to be equal to 10^{-14}. If an integration ends in a complicated region, it will start the next integration using a small timestep, so that it does not attempt to work through a complicated region using too large a stepsize. However, if the integration ended in a non-complicated region, the error program will simply build the size of h back up from h_0, with no loss of accuracy and a minimal increase to the total computation time.

Four parameters are required to determine how data is printed and the length of the integration. The size of each integration T_{inc} must be specified. The size of this value is arbitrary, as long as it is not too large. Very large values risks the computer running out of memory before the simulation is complete. If that occurs, the program will break and you will lose *all* of the data from that particular integration. I will use $T_{inc} = 10000$ timesteps unless otherwise specified. The initial time determines what the integration labels the starting point. I will always use $t_i = 0$. The number of integrations will determine the length of the integration. For example, if you wanted 100 integration runs, then *ResCap* will integrate to $t_f = 10000 \cdot 100 = 10^6$ yr.

When each smaller integration is complete, *ResCap* runs a data program that takes the 12 variables at each timestep (15 if we are including mass accretion), and makes several calculations that are printed to a data file. These can include the semi-major axis of each planet, the energy of the system, etc. This method also allows us, in the case of a collision or other event where *ResCap* would break, to have data up until that event.

Finally, since the timestep can be increasingly small ($<< 1$), all the data points are not necessary. By specifying t_{pnt}, you state that in the data file, *ResCap* will print one data point every t_{pnt} timesteps. By increasing t_{pnt}, you can greatly reduce the size of the data file, but making its value too large risks losing valuable information. Unless specified, I will use $t_{pnt} = 1$.

Collision Detection

Currently a collision detection algorithm is being developed to allow for the possibility of physical collisions to occur without *ResCap* breaking. It will not be necessary for the current results, but will allow for additional tests on the configuration of planetary systems in discs. The general idea is as follows. At each timestep, *ResCap* will measure the relative distances between the point masses. If the relative distance is within a predetermined value, it will log that a collision occurred. It will then replace the two particles with a single particle that has the same mass and linear momentum as the original pair. Modeling has shown that collisional fragmentation does not occur on large scales ($< 10\%$), and remmant ejections are not significant to the subsequent evolution of the system (Alexander & Agnor 1998).

3.3 Initial Tests

If we allow the f^j terms in Equations 3.26 to be 0 for all j, we have a conservative system. I will use conservative systems to test *ResCap* in order to ensure that everything is working properly before we begin to include migration and external effects. Also, using a conservative system, we can test the error buildup in both the total energy and total angular momentum at various Δ_0. Additionally, we will compare the computational time required to achieve such accuracies to determine the value of the error parameter, Δ_0.

The Center of Mass

A good initial test is to make sure the center of mass remains close to the origin. We cannot expect it to be fixed at the origin due to roundoff errors, but should expect the velocity of the center of mass to by incredibly small. I will define the system to be a solar star and two Jupiter-mass planets, placed on circular orbits. Figure 3.1 plots the x and y components of the center of mass's velocity for two integrations: one with the location of the planets arbitrarily selected, and one where they are in a 2:1 resonance. As we see, the velocity never exceeds changes greater than 10^{-14} over long timescales. Every integration would give a different result,[7] but each would be on the same order of magnitude, whether in resonance or not.

[7] Remember, the location of the outer planet on its orbit is randomized, so we would expect the motion to be different on these small scales.

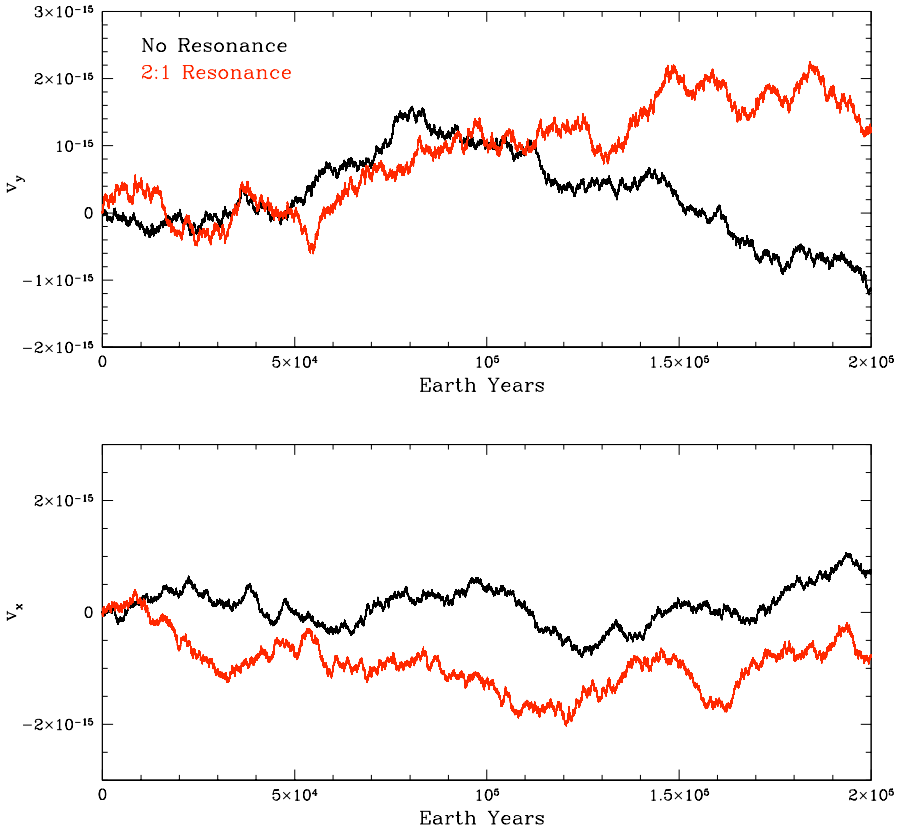

Figure 3.1: The y and x components (in $\tilde{L}\tilde{T}^{-1}$, *top* and *bottom* panels, respectively) of the center of mass's velocity in a conservative system. We see that it remains neglibigble, and fluctuates due to small oscillations and roundoff errors.

Orbital Parameters Remain Fixed

Additional tests include using both a simple two-body system and a configuration from our Solar System. For the two-body system, there are no perturbations on the binary system from additional objects, so we should expect the orbital parameters of the planet to remain fixed over long timescales. Below in Figure 3.2 is a (somewhat uninteresting) plot of a Jupiter-mass planet orbiting a solar star. I have given the planet an initial non-zero eccentricity. In the upper panel, we see that the semi-major axis does not change over time, while the lower panel shows the eccentricity remains fixed. The changes in the semi-major axis and eccentricity are no greater than one part in 10^4. Additionally, I plot Jupiter and Earth and allow the integration to run for $5 \cdot 10^5$ yr. We see in Figure 3.3 that the orbital parameters do not change over long timescales. The plots on the left panels show that the semi-major axes and the ratio of the orbital periods are stable, while the plots on the right panels show that the eccentricities (initially zero) remain fixed to one part in 10^3.

3.3.1 Errors: Determining Δ_0

We can now test the error buildup for *ResCap* in order to determine the value of Δ_0 to be used for *ResCap*. Also, we must make sure that the accuracy is independent of the particular integration. What I mean is that no matter what we are simulating, whether the planets are close together or far apart, we should arrive at similar error buildups. We can test this by setting up three-body systems at various resonances. The resonances will determine how close the planets are to each other, and therefore the strength of the mutual perturbations. I will set the masses of both planets to be Jupiter-mass planets, so that the mutual perturbations are not strong enough to cause the system to go unstable. I will then allow *ResCap* to integrate for $5 \cdot 10^4$ timesteps, with Δ_0 set to $10^{-\alpha}$, where α is a positive integer between 10 and 18. The error buildup for energy and angular momentum is linear, so I will then extrapolate the error to larger timescales (10^7 yr). For these simulations I will use, in order of increasing separation, the 3:2, 2:1, and 3:1 resonance. Additionally, I will use two configurations where the planets are not in a particular resonance, one placing the planets slightly above the 3:1 resonance, and one with large separation (the ratio of the periods is ~ 9.5.) The results are plotted below in Figures 3.4 and 3.5. We see that for a given Δ_0, the error buildups for energy and angular momentum stays within one order of magnitude of each other regardless of the system configuration. This justifies that the accuracy parameter is independent of the configuration of the system in the integration, as desired. A linear fit is observed for $\Delta_0 \leq 10^{-16}$, but both energy and angular momentum experience a divergence from this linear fit beyond that point. Recall Figure 3.1, where the scale was on the order of 10^{-15}. Therefore, the measurements beyond 10^{-15} are a result of the small oscillations in the motions of the system, and cannot be taken seriously. Therefore, if we want to demand high accuracies, but not high enough so that we are dealing with the small oscillations of the system, we

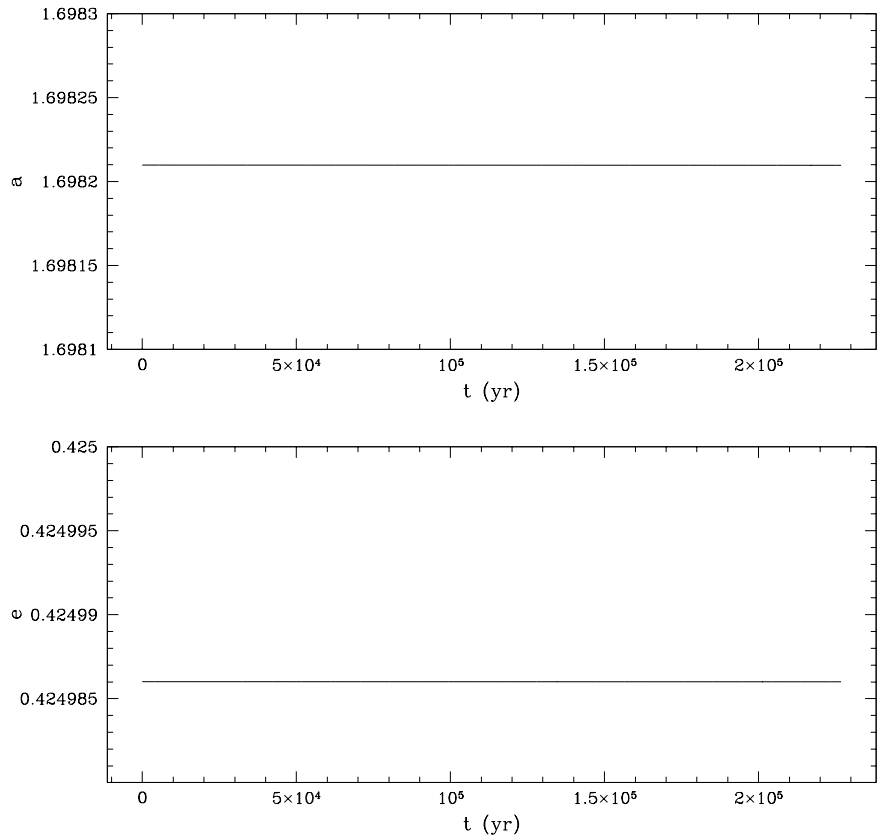

Figure 3.2: The semi-major axis (in AU, *top panel*) and the eccentricity of a 1 M_J planet around a 1 $M_\odot$ star. (*bottom panel*).

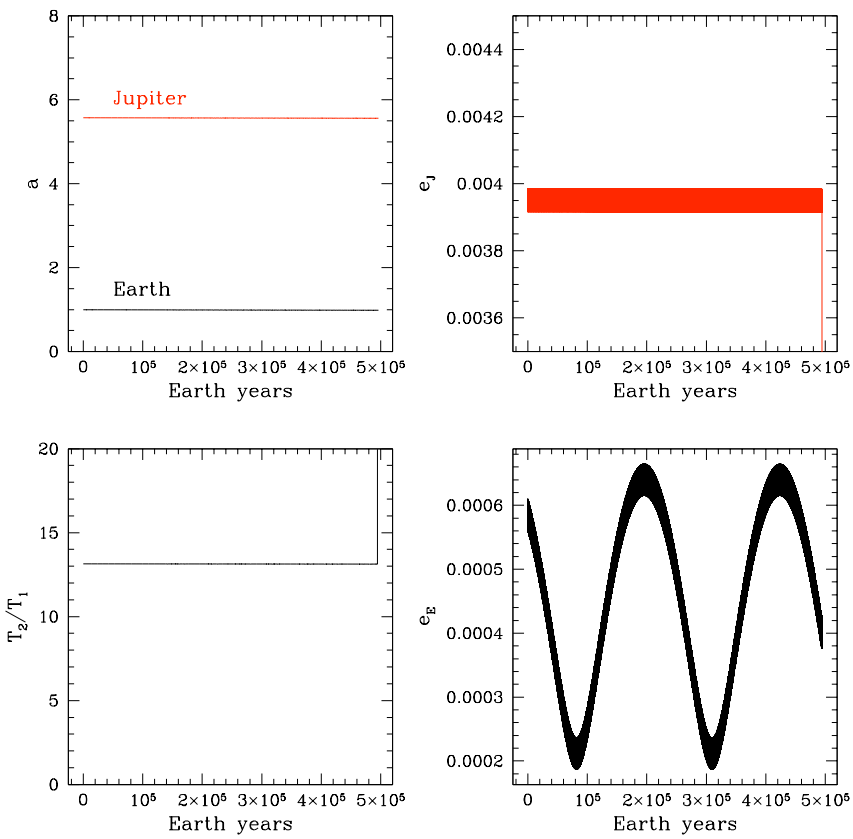

Figure 3.3: *Top-Left Panel:* The semi-major axes of Jupiter and Earth (in AU). *Bottom-Left Panel:* The ratio of orbital periods of Jupiter and Earth. *Right Panels:* The eccentricity of Jupiter and Earth (*top* and *bottom* panel, respectively).

should restrict ourselves to the regime where

$$-\log_{10}(\Delta_0) \leq 16. \tag{3.28}$$

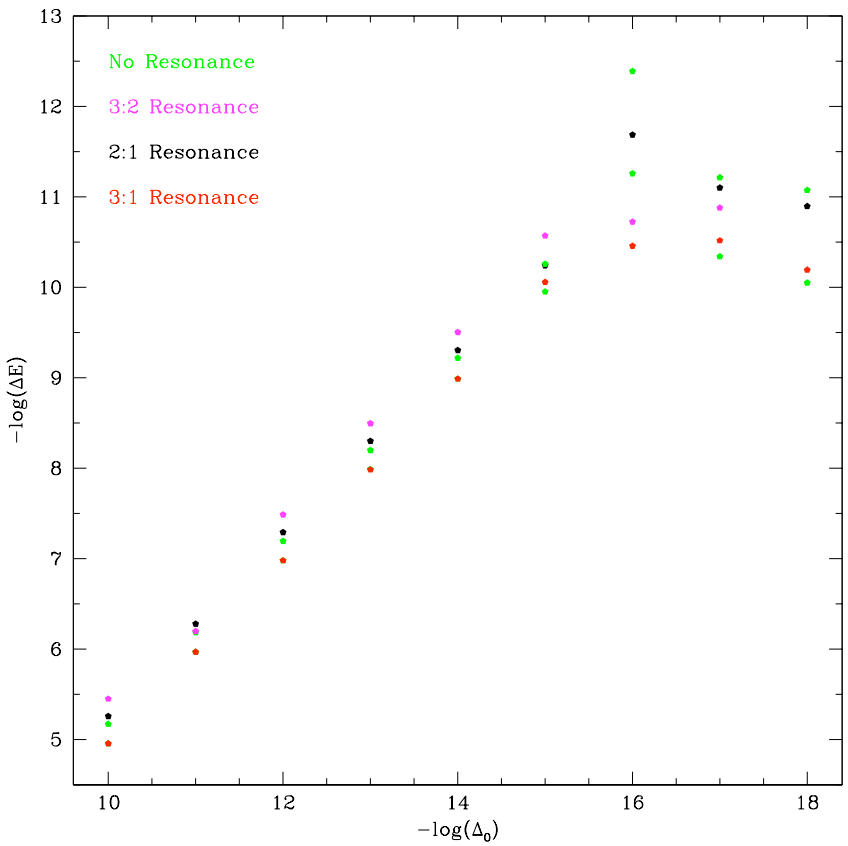

Figure 3.4: Error buildup for the total energy, ΔE, after 10^7 timesteps.

However, demanding exceedingly high accuracies can lead to increased computational time. In order to select the accuracy parameter, I will log the computational time *ResCap* takes to integrate two Jupiter-mass planets in 2:1 resonance for 10^5 timesteps at various Δ_0. For each run, the print statement will be ignored, so we are comparing only the time it takes to integrate the equations of motion. The additional time necessary for printing is minimal for these integrations, and can be safely ignored in the comparison. The results are plotted below in Figure 3.6. We see there is an expodential increase in the computation time for each additional power of Δ_0 that we demand. However, we can

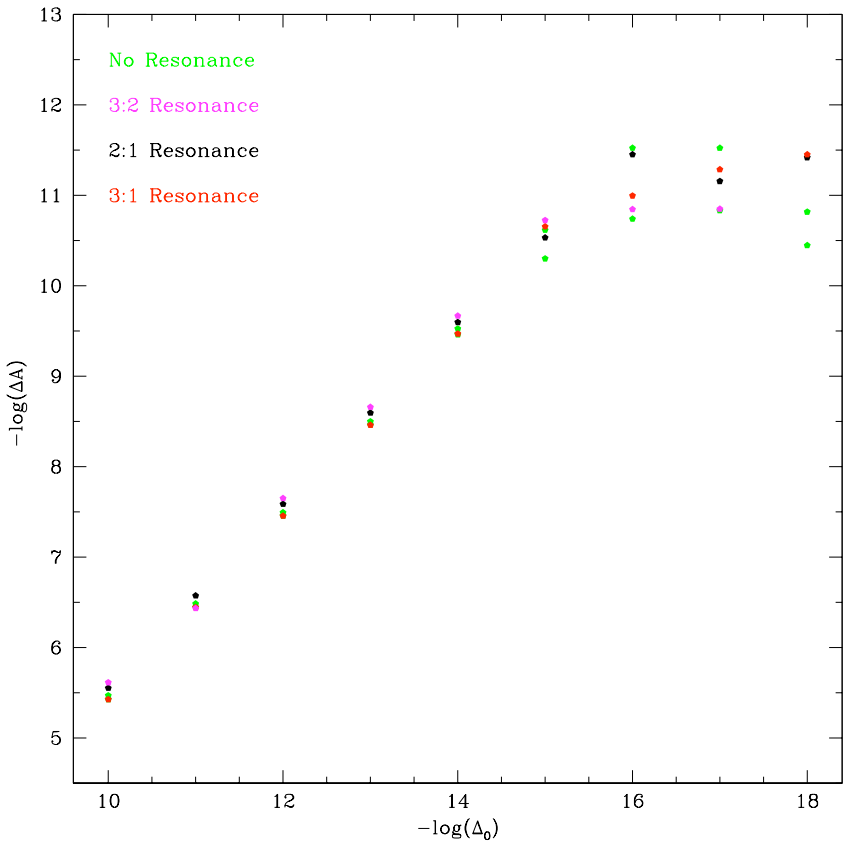

Figure 3.5: Error buildup for the total angular momentum, ΔA, after 10^7 timesteps.

keep long integrations under 20 hours as long as we restrict $-\log_{10}(\Delta_0) \leq 14$. Therefore, I will select $\Delta_0 = 10^{-14}$ as my accuracy parameter for *ResCap*.

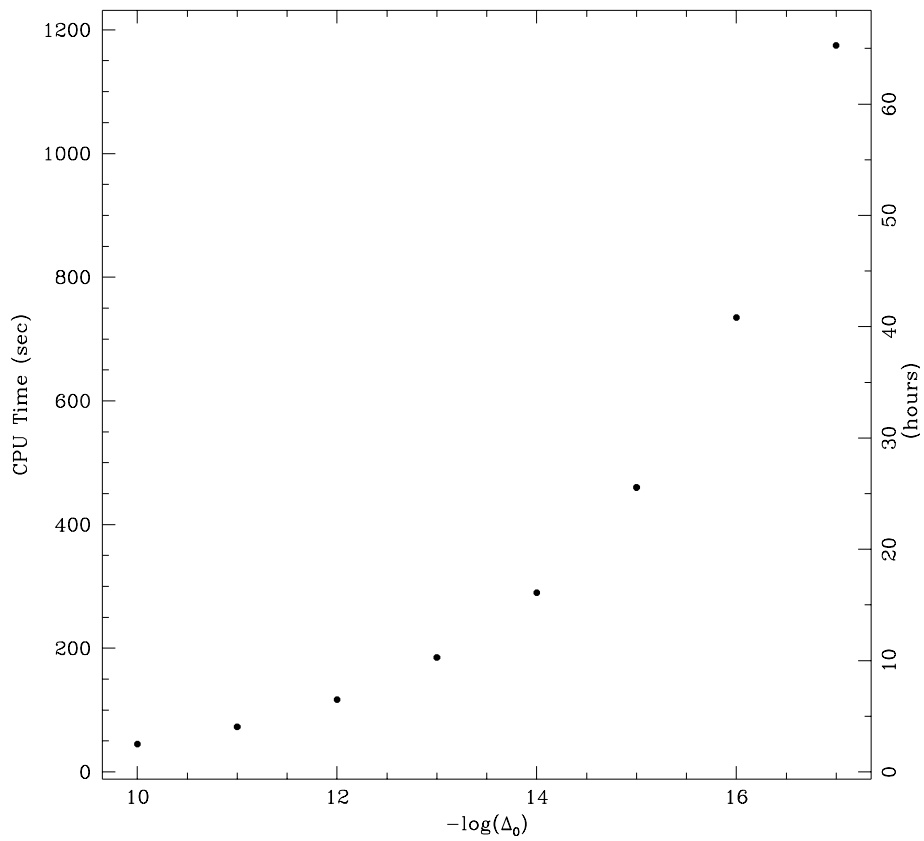

Figure 3.6: Computational Time versus the accuracy parameter, Δ_0. The left axis measures the time (in seconds) to calculate $5 \cdot 10^5$ timesteps. The right axis (in hours) extrapolates this to the amount of time it would take to run for 10^7 timesteps.

3.4 Migration

The additional terms f_x^j in Equations 3.26 control the migration of the planets. For these integrations, I will be allowing the outer planet to be the only planet that migrates. My justification is that these simulations will assume that the massive planet is large enough (typically of Jupiter size) so that it has opened

a gap in the protoplanetary disc. Therefore, the scarce presence of gas within this gap has a negligible effect on the inner planet. The outer planets will typically be of Earth-mass size, and so are not small enough to have opened an appreciable gap.

The migration will be incapsulated by two terms, a migrational term and an eccentricity damping term. The migrational term is the standard friction term proportional to the velocity of the planet,

$$\mathbf{a}_{mig} = -\alpha \mathbf{v}, \tag{3.29}$$

where α is a positive constant with units of s^{-1}. It will be convienient for us to write α as $1/t_{mig}$, a value we will call the *migration timescale*. The eccentricity damping term is proportional to the radial direction of the planet, and is meant to circularize eccentric orbits. It is of the form

$$\mathbf{a}_{ecc} = -2\beta \frac{(\mathbf{v} \cdot \mathbf{r})\mathbf{r}}{r^2}. \tag{3.30}$$

Again, we will write β–a constant with units of s^{-1}–as $1/t_{ecc}$, which we call the *damping timescale*.

The form of t_{mig} and t_{ecc} will be of interest to us. For these integrations, we will use two particular models. One model, hereafter the constant value model, will fix the values of t_{mig} and t_{ecc} throughout the integration. The values will be selected to mimic previous models of protoplanetary discs. This is a general form of modeling friction in discs, and is not restricted to any particular mass range. The other model was developed in Papaloizou & Larwood (2000), which directly takes into account various parameters of the disc. In particular these timescales are important when the eccentricity of the planet exceeds the aspect ratio of the disc, H/r, where H is the disc height. It is in these situations they have shown that eccentricity can help to prevent further inward migration, and can actually lead to outward migration. The form of the timescales are the following:

$$\begin{aligned} t_{mig}(yrs) &= 3.5 \times 10^5 \left[\frac{1 + (e_o a_o/1.3H)^5}{1 - (e_o a_o/1.1H)^4}\right] \left(\frac{H/a_o}{0.07}\right)^2 \left(\frac{\Sigma}{588\ \mathrm{gcm}^{-2}}\right)^{-1} \\ &\quad \times \left(\frac{M_o}{1M_E}\right)^{-1} \left(\frac{a_o}{1\ \mathrm{AU}}\right)^{-1/2} \end{aligned} \tag{3.31}$$

$$\begin{aligned} t_{ecc}(yrs) &= 2.5 \times 10^3 \left[1 + \frac{1}{4}\left(\frac{e_o}{H/a_o}\right)^3\right] \left(\frac{H/a_o}{0.07}\right)^2 \\ &\quad \times \left(\frac{\Sigma}{588\ \mathrm{gcm}^{-2}}\right)^{-1} \left(\frac{M_o}{1M_E}\right)^{-1} \left(\frac{a_o}{1\ \mathrm{AU}}\right)^{-1/2}, \end{aligned} \tag{3.32}$$

where Σ is the density of the disc. You can see when e exceeds the aspect ratio of the disc in the t_{mig} formula, the denominator of the [ ] factor becomes negative. These formulae, however, assume that the planet is of planetesimal size, and therefore are only valid under the rough upper limit of 100 M_E.

Chapter 4

Results

ResCap was developed in order to better understand resonant interactions in a protoplanetary disc and to gain a more general understanding of which parameters have dominant roles for the long-term evolution and stability of planetary systems. In this chapter I will summarize some of the results that I have been obtained with *ResCap*.

4.1 Migration and Eccentricity Damping

Recall the form of the friction term that will govern the migration of the outer planet:

$$f = -\frac{\mathbf{v}}{t_{mig}} - 2\frac{(\mathbf{v}\cdot\mathbf{r})\mathbf{r}}{r^2 t_{ecc}}. \tag{4.1}$$

The first term controls the rate at which energy is dissipated from the outer planet, and hence controls the rate of inward migration. Let us explore this term some more. I will eventually adopt a value of 20,000 yr for t_{mig}. While it should be no surprise that smaller t_{mig} corresponds to faster migration, recall that resonance can slow the rate of inward migration. How much does migration slow, and what factors determine this? Consider a 2:1 resonance with two Jupiter-mass planets. I place the outer planet slightly beyond the 2:1 resonance and allow it to migrate (without eccentricity damping) and capture the inner planet. The two planets then migrate as a coupled system. The outer planet's semi-major axis for various values of t_{mig} is plotted below in Figure 4.1. Comparing the slope prior to resonance trapping to the slope after capture, the rate of migration slows by roughly a factor of three, independent of the value of t_{mig}.

The timescale for planet migration is the disc viscous timescale, which Ward (1997) determined to be

$$\frac{1}{t_{mig}}\ (\mathrm{yr}^{-1}) = \left|\frac{\dot{a}}{a}\right| \approx \frac{3\nu}{2a^2} = \frac{3}{2}\alpha(H/a)^2\Omega = 5.3\times10^{-5}\left(\frac{\alpha}{4\times10^{-3}}\right)\left(\frac{H/a}{0.05}\right)^2$$

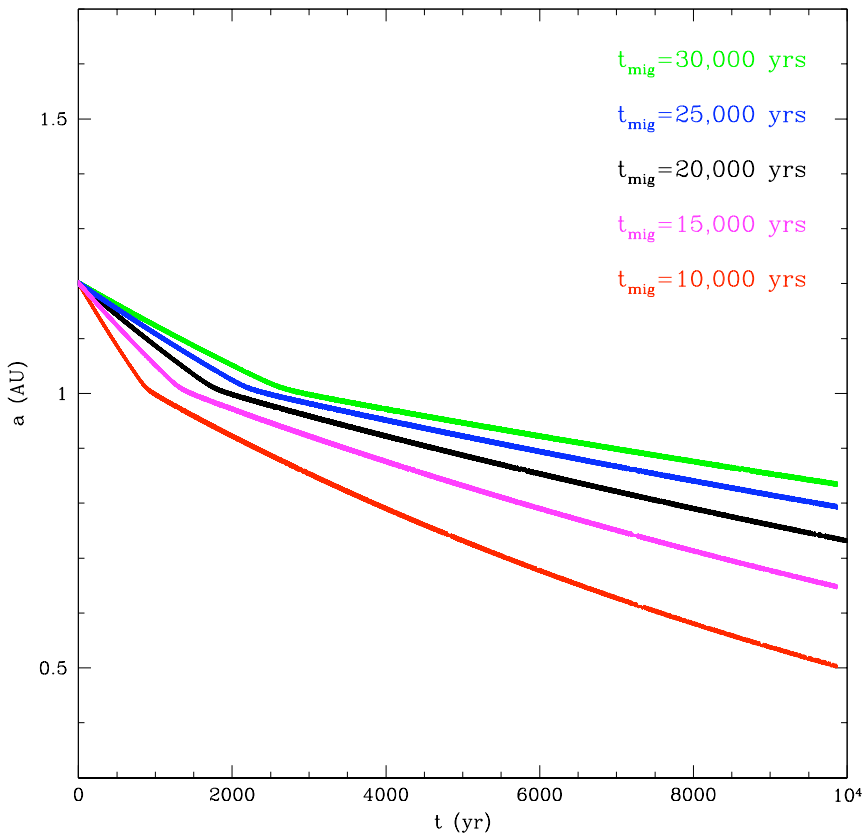

Figure 4.1: Various rates of migration for a 1 M_J planet. The location where the planet is in a 2:1 resonance with the 1 M_J inner planet (not plotted) is at 1 AU.

$$\times \left(\frac{M_o}{0.32 M_{Earth}}\right)^{1/2} \left(\frac{a}{1AU}\right)^{3/2} \tag{4.2}$$

where ν is the viscosity, H is the disc height, Ω is the Keplerian angular velocity, and α is a constant. This is similar to the result in Papaloizou and Larwood (2000). However, much can be understood by allowing this to be a simple constant. Observations of T Tauri discs have shown that $\alpha \sim 10^{-2}$, and $H/a = 0.05$ (Bryden et al. 2000; Kley 2000; Papaloizou et al. 2001). Using $a = 1$ AU for Earth-mass planetesimals, we get $t_{mig} \sim 20,000$ yr. Unless specified, when I use the constant value model, I will use $t_{mig} = 20,000$ yr. Also, r_{res} will be assumed to be set to 1 AU.

Figure 4.1 shows that the factor by which migration is slowed does not depend on the value of t_{mig}. Let us further compare this factor with the mass of the outer planet. Again, I will use a Jupiter-mass inner planet, but fix t_{mig} at 20,000 yr. The results are shown in Figure 4.2. We see that the mass of the outer planet, where the friction is applied, does affect the rate of migration for the "coupled system." If $M_o << M_i$, then the rate at which energy is dissipated is significantly less than would be the case if the outer and inner planets had comparable mass. A plot of the ratio of these migration rates can be observed in Figure 4.3. The migration change factor is large when $M_0 << M_i$ and approaches unity as $M_o \rightarrow M_i$. This shows a strong relation between the change in the migration rate and the outer planet for masses less than a mass of the inner planet.

The eccentricity damping term is meant to circularize eccentric orbits in contrast to resonances, which can induce eccentricities in both bodies. Figure 4.4 shows a simple example with two Jupiter-mass planets locking into a 2:1 resonance (without eccentricity damping in Equation 4.1). While the eccentricities remain small, once resonance is hit, there is a sudden increase in eccentricity. Without damping, this would grow continuously until instability occurred.

In addition to the migrational effects tidal interactions can have on the planets, these interactions can also affect the planets' orbital eccentricities (e.g., Goldreich & Tremaine 1980; Artymowicz 1992, 1993; Papaloizou et al. 2001). A planet interacts with the disc in the vicinity of its Lindblad and corotation resonances–where the mean motion and secular resonances occur simultaneously. The nearby corotation resonances of the planet produce the greatest effect on $\dot{e}$. Likewise, the Lindblad resonances excite eccentricity in the planet (Goldreich & Sari 2002). In the presence of disc material the net effect is eccentricity damping.

Now, how do we define t_{ecc}? For the constant value model, we will use the form $t_{ecc} = K t_{mig}$, where K is a positive constant (≤ 1). The justification for this can be seen by comparing the equations from Goldreich & Tremaine (1980), where Δ is the width of the gap formed by the planet, with $\Delta << a$,

$$\left|\frac{\dot{e}}{e}\right| = 0.116 \left(\frac{M}{0.32 M_\odot}\right) \left(\frac{\Sigma a^2}{0.32 M_\odot}\right) \left(\frac{a}{\Delta}\right)^4 \Omega, \tag{4.3}$$

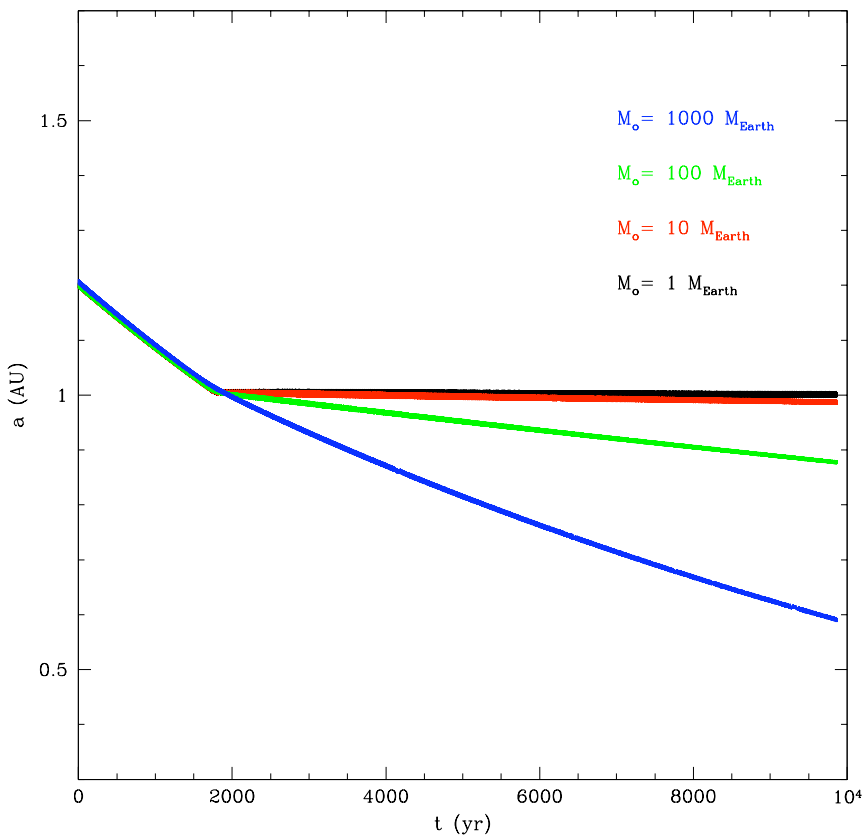

Figure 4.2: Rates of migration after resonance trapping for several masses of the outer planet. The location where the planet is in a 2:1 resonance with the inner planet (not plotted) is at 1 AU.

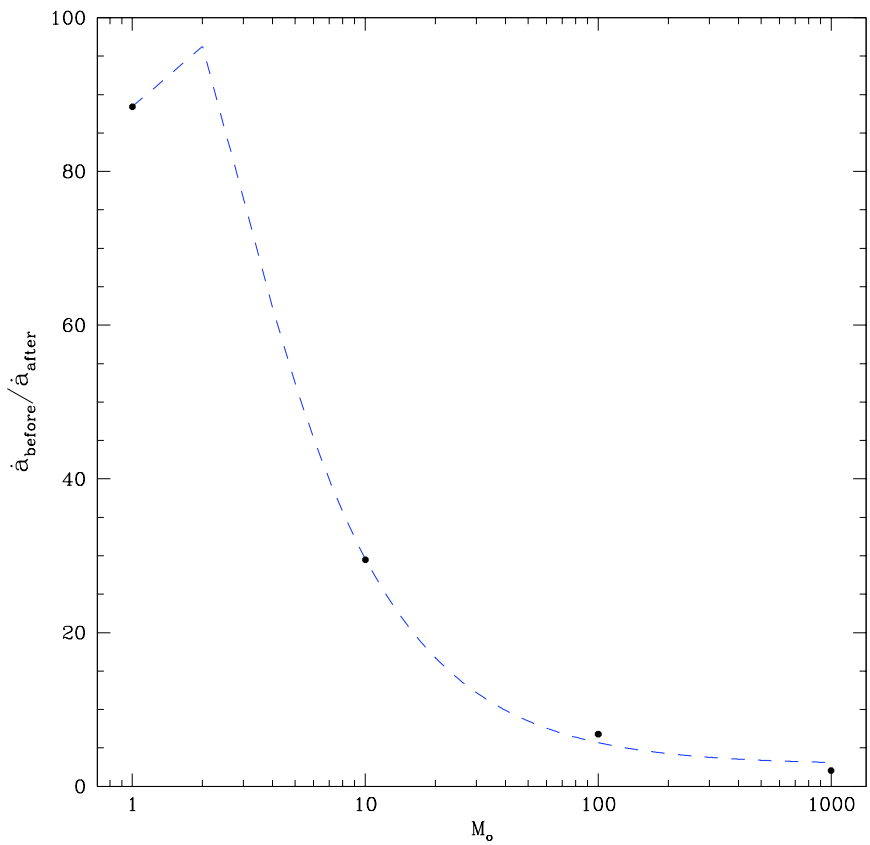

Figure 4.3: Ratios of the rates of migration from Figure 4.2. A least-squares fit to the functions $\{1, 1/M, 1/M^2\}$ is plotted in blue.

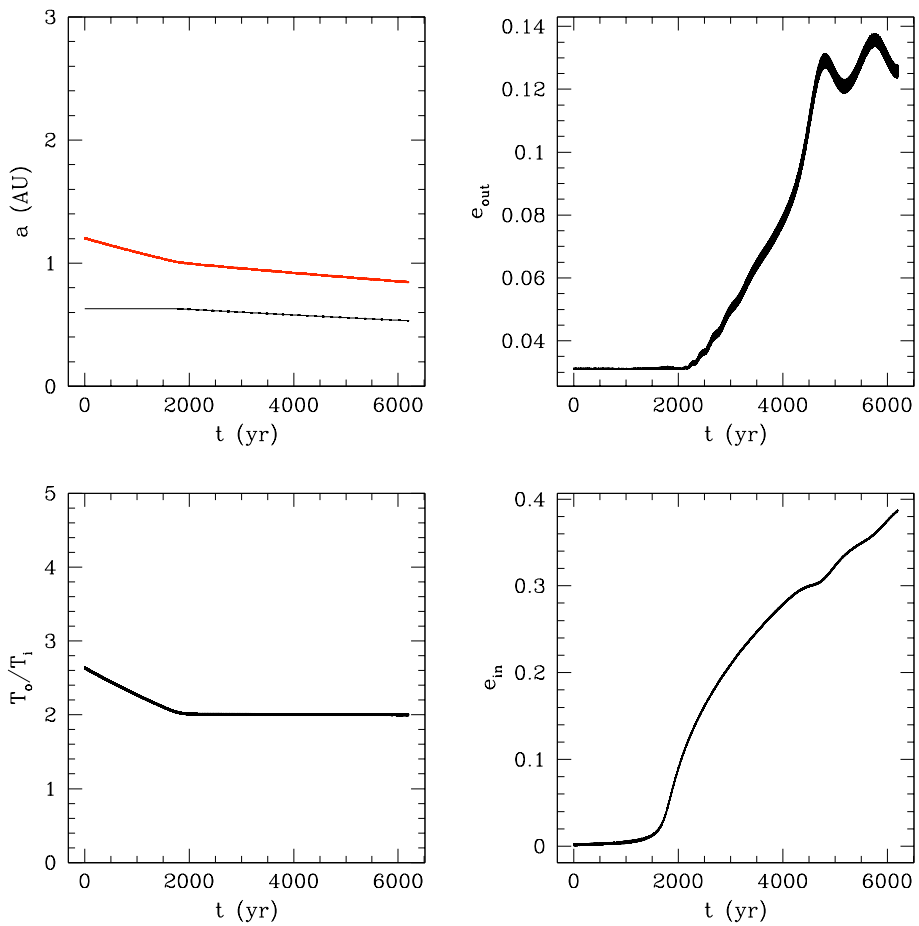

Figure 4.4: Two Jupiter-mass planets locking into a 2:1 resonance. Their semi-major axes are plotted (in AU) on the top-left panel. The ratio of their orbital periods is plotted in the bottom-left panel. Once trapped at $\sim$ 2000 yr, the initially circular orbits gain eccentricity (shown in the right panels).

$$\left|\frac{\dot{a}}{a}\right| = 1.67\left(\frac{M}{0.32M_\odot}\right)\left(\frac{\Sigma a^2}{0.32M_\odot}\right)\left(\frac{a}{\Delta}\right)^3\Omega, \tag{4.4}$$

and noting that $\dot{e} = \gamma\dot{a}$. This form of eccentricity damping has the convenient property that the eccentricities reach equilibrium values after capture in resonance for arbitrarily long timescales. This occurs when the damping balances the excitation due to resonant interaction between the planets.

Consider the 2:1 and 3:2 resonances. We will examine the parameter space for $M_o \in \{1M_E, 10M_E, 100M_E, 1M_J\}$, $K \in \{1, 0.1, 0.01\}$, and $t_{mig} = 20,000$ yr, measuring the final eccentricities gained by the planets after resonance trapping has occurred. The criterion for this is to have *ResCap* record the final eccentricity once $\dot{e}$ no longer changes to within 1% its value. The results are shown in Figure 4.5. Several trends are clear:

- Lower mass outer planets are unable to produce high eccentricities in the inner planet, regardless of the value of K.
- Massive outer planets tend to produce higher eccentricities in the inner planet.
- Larger values of K typically produce higher final eccentricities in both planets.
- The final eccentricities for the inner planet in the 3:2 resonance are generally a factor of three smaller than the final eccentricities of the inner planet in the 2:1 resonance. Similarly for the outer planet.

4.2 Can Eccentricity Save Planets?

One problem facing theories of planet formation is runaway migration. All theories suggest that most planets formed in discs will migrate until they either collide with the star or are ejected through strong gravitational perturbations. Papaloizou & Larwood (1999) investigated how small eccentricities alter the effects of the Lindblad and corotation resonances on the protoplanet. Their results culminated with Equations 3.31. We now compare this model for t_{mig} and t_{ecc} with the constant value model.

For the simulations using Papaloizou and Larwood's model, I adopt the following values for the density and scale height of the disc (Thommes 2005):

$$\begin{aligned} \Sigma &= 1000\left(\frac{r}{1\ \mathrm{AU}}\right)^{-1}\ \mathrm{g\,cm^{-2}} \\ H &= 0.03\left(\frac{r}{1\ \mathrm{AU}}\right)^{5/4} r, \end{aligned} \tag{4.5}$$

where r is the radial distance from the star. For the constant value model, I use $t_{ecc} = 0.1t_{mig}$. Figure 4.6 is a clear example of the difference between this model and the constant value model. Notice that resonance pumps up

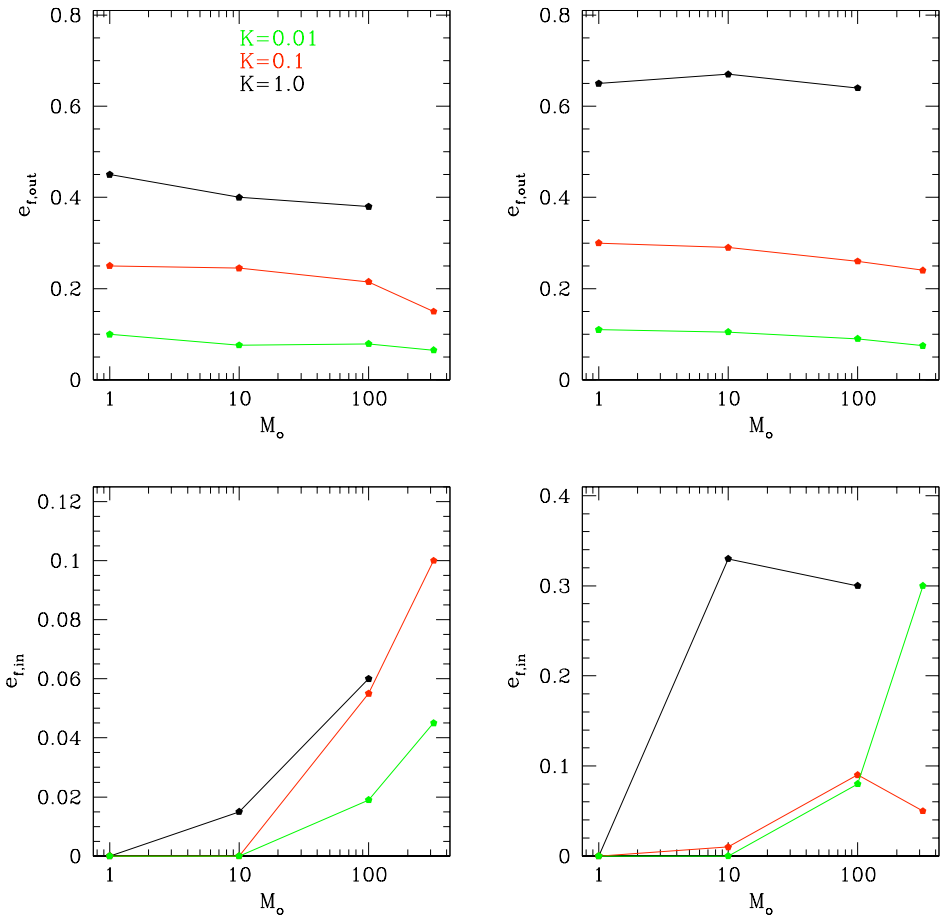

Figure 4.5: The final eccentricities for various values of K in $t_{ecc} = Kt_{mig}$. The mass of the inner planet is fixed at $1M_J$, and M_o is the x-axis. *Left Panels:* Final eccentricities for the 3:2 resonance for the outer and inner planet (*top* and *bottom* panels, respectively). *Right Panels:* Final eccentricities for the 2:1 resonance for the outer and inner planet (*top* and *bottom* panels, respectively). Omitted points signify that instability occurs before an equilibrium value can be reached.

eccentricity until migration reverses and the outer planet migrates *out* of the resonance (*top-left panel*). At this point, the resonance can no longer pump up eccentricity, and damping brings it back down (*top-right panel*), reversing the migration direction again.

This eccentricity mechanism can serve as a means to prevent the planets from migrating into the star on short timescales. Once the outer planet leaves resonance, the planets no longer move as a coupled system and energy is not dissipated from the inner planet, which prolongs its orbital lifetime. Figure 4.7 compares the migration rates for 1 M_E, 10 M_E, and 50 M_E in the *top-left*, *top-right*, and *bottom-left panels*, respectively. We see that for massive planets, Papaloizou and Larwood's model caused the migration to be so rapid that the 2:1 resonance was skipped and the planet later locked into the 3:2 resonance. Overall, the migration rate was not slowed, but rather increased! For the 10 M_E planet, we see that the rate of migration in the non-constant model eventually equals the constant value model and is unable to serve as a means to slow migration. However, for Earth-mass planets, the migration rate is significantly slowed. Therefore, this model serves as a way to prevent migration of smaller protoplanets and small Earth-size planets in discs where a giant planet has formed a gap. However, comparing with our solar system, we see the small Earth-like planets are *inside* the orbit of the gas giants. By what mechanisms could the planets "switch places?" Dynamical instability proposes itself as one such answer, which will be explored in Section 4.4.

4.3 Mass Limits on Resonance Trapping

For the majority of this chapter, I have been using the 2:1 resonance, with several comparisons to the 3:2 resonance. My selection was not arbitrary. For the previous results, the comparisons relied on the fact that resonance capture *had* occurred. We never had to be concerned with the outer planet *passing* the resonance location during its migration. The 2:1 and 3:2 resonances are first-order resonances, that is, $\Re = (p + 1) : p$. They have the characteristic that resonance trapping occurs readily as long as (1) the migrating planet is not massive enough, or (2) the planet is not migrating too fast through the resonance location. We explore part of this parameter space here in the low-eccentricity regime. For these simulations, I will use the constant value migration model, with $t_{ecc} = 0.1t_{mig}$. The setup is as follows: The planets are arranged so the outer one is outside the resonance, allowing a distance between 0.1-0.2 AU to migrate until it reaches the resonance location. Then, a catalog will be made whether resonance capture occurred. If capture occurred, the outer planet is increased by a half order of magnitude (1, 5, 10, 50, 100, 500, ...) in Earth-masses, and the process will continue until trapping does not occur. Additionally, when capture does not occur, it is be logged whether it *passed* the resonance location, or whether dynamical instability caused the system to dissipate. The inner planet will remain a Jupiter-mass planet throughout. In addition, eccentricity will be initially given to the outer planet in some of the integrations. I will

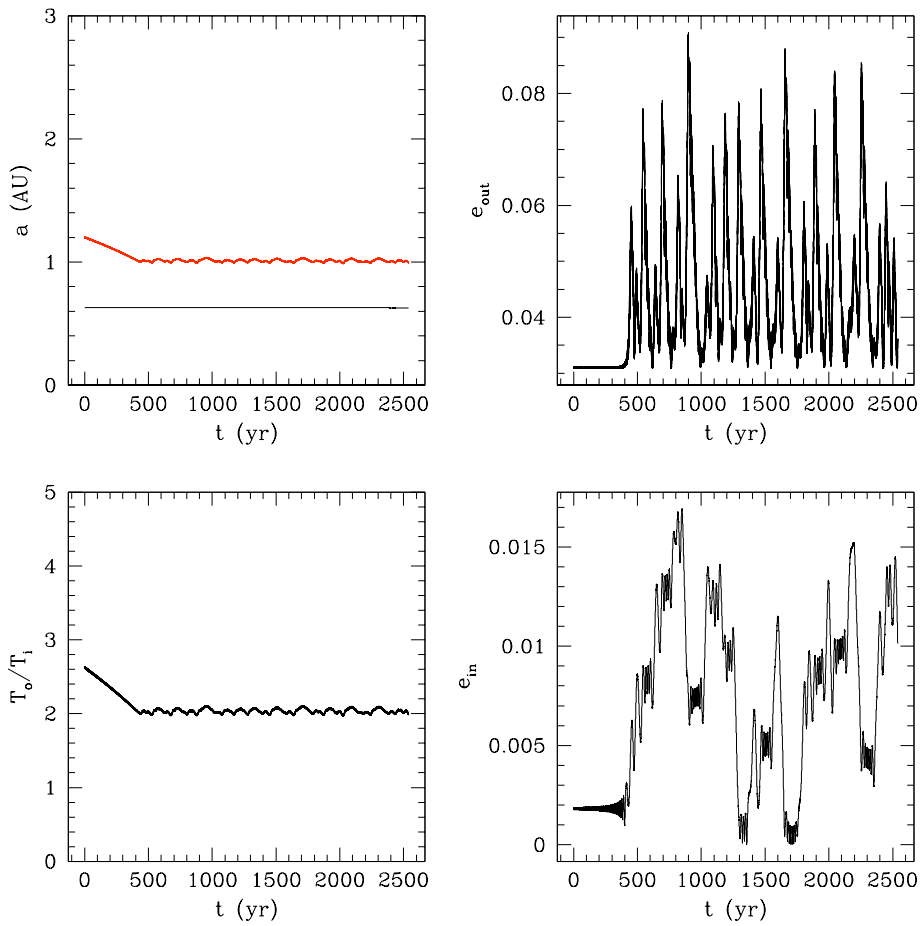

Figure 4.6: Orbital migration of a 10 M_E planet using Papaloizou and Larwood's model for t_{mig} and t_{ecc}. *Top-Left Panel:* A plot of the semi-major axes (in AU) of the planets. The 2:1 resonance serves as a *barrier*: once the planet is in resonance, eccentricity pumping occurs (*top-right panel*) and results in outward migration. Without resonance to excite eccentricity, damping reduces the eccentricity of the planet until the migration reverses direction.

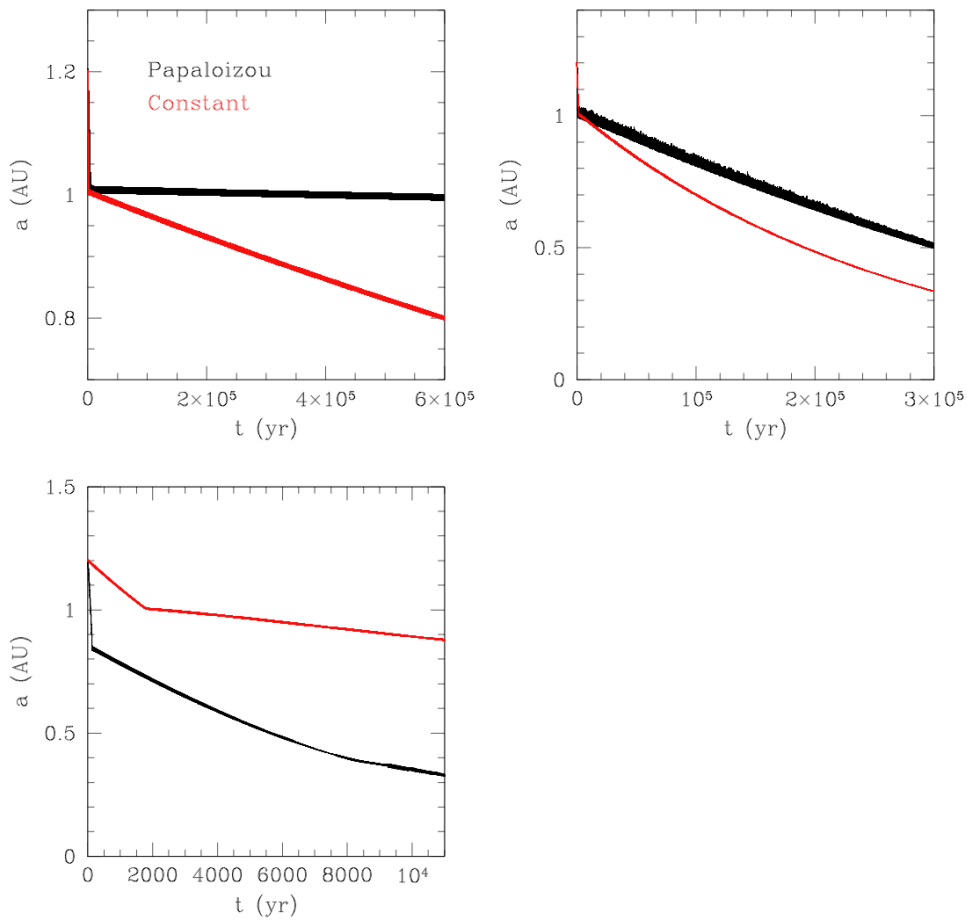

Figure 4.7: The semi-major axis of the outer planet during resonance trapping with a 1 M_J inner planet (not shown), using either the constant value model or Papaloizou's model for the migration and eccentricity timescales. The mass of the outer planet is 1 M_E, 10 M_E, and 50 M_E for the *top-left, top-right, and bottom-left panels*, respectively.

take the initial eccentricities to be either zero or 0.2. Since damping is present, the eccentricity at resonance is between 0.1 and 0.15. The resonances we will consider will be the 2:1, 3:2, 4:3, 5:4, 3:1, 5:3, 4:1, 5:2, and 7:4. The results are summarized in Table 4.1. Several trends are immediate:

- The first-order resonances are more stable than the second or third-order resonances at low eccentricities.
- For all the first-order resonances, the maximum mass is limited by dynamical instability. We only see the outer planet passing the resonance location in the 3:1 (second-order), and third-order resonances.
- Eccentricity greatly limits the mass limit of every resonance except the 5:2. Failure for any resonance captures to occur in, for example, the 3:1 resonance, relied on the fact that the eccentricity of the outer planet is still small. Simulations have shown that planets with high (> 0.6) eccentricities are capable of being captured into the 3:1 or 4:1 resonance. We will see some examples below.

$M_* = 1\ M_\odot$, $M_i = 1\ M_J$,									
e_o	2:1	3:2	4:3	5:4	3:1	5:3	4:1	5:2	7:4
0	10000*	1000*	0*	0*	0	1000*	0	0	1000
0.2	50*	0*	0*	0*	0	0*	0	10	0*

Table 4.1: For a given resonance and eccentricity, the minimum mass (in M_E) where resonance trapping did not occur. A '*' signifies that resonance trapping failed due to dynamical instability, rather than the planet migrating past the resonance location.

4.4 Dynamical Instability: A Way to Make Eccentric Planets?

Rasio & Ford (1996, 2007) have shown that dynamical instability can produce large eccentricities consistent with observed extrasolar planets. Knowing how often and under what conditions this occurs would help to better understand the process of planet formation and in determining whether systems are stable or not. It is important to determine how often this occurs along with the necessary conditions necessary to produce close interactions with the planets. This part of the study is currently still on going, but a few results are already apparent. Particular resonances allow for dynamical instability more readily than others. This can be analyzed analytically. Compare the 3:2 resonance with the 2:1 resonance. First, the 3:2 resonance brings the planets closer together in comparison with the 2:1, so large-mass planets would have a better chance to mutually perturb each other. This can be shown from the discussion in Chapter

3: for resonances of the form $\Re = (p+1) : p$, the separation in the semi-major axis, Δa is estimated as

$$\Delta a \cong \frac{2}{3}\frac{1}{p^2}a_o. \tag{4.6}$$

Therefore, Δa decreases with increasing p. Additional relations for other resonances can be determined. Continued simulations cannot produce any possible configurations where an outer planet can move into a 2:1 resonance and become dynamically unstable so that one of the planets survives in the end. Typically, a collision occurs because the 2:1 resonance requires the mass of the planets to become unrealistically large. However, the 3:2 resonance allows for such configurations. Figure 4.8 gives one such example of two Jupiter-mass planets in the 3:2 resonance becoming dynamically unstable. The outer planet switches places with the inner planet, leaving the inner planet on an eccentric orbit.

The previous section gives several additional examples of dynamical instability creating eccentric orbits. With a 1 M_J inner planet, the 3:2 and 5:4 resonances are dynamically unstable. That is, planets in this resonance with a Jupiter-mass planet are within the sphere of influence of the Jupiter, the regime where dynamical instability can occur. This region is approximated by the Hill sphere, which has radius

$$r_{Hill} \cong \left(\frac{M_i + M_o}{3M_*}\right)^{1/3}\left(\frac{a_i + a_o}{2}\right) \tag{4.7}$$

for circular orbits. Thus, if orbits fall within several Hill spheres of the body, the gravitational influences can become large. For a Jupiter-mass orbiting a 1 $M_\odot$ star at ~ 0.8 AU with a third planet located at ~ 1.2 AU, the Hill radius is $r_{Hill} \sim 0.03$ AU. This may seem small, but if the body near 1.2 AU has an eccentricity of 0.3, the semi-*minor* axis is $a(1-e) = 0.84$ AU, placing it very close to the Hill sphere. I observed that most planets become gravitationally unstable in the cases where the outer planet initially had non-zero eccentricity. Figure 4.9 is one such example. A 1 M_E planet with ~ 0.3 initial eccentricity (*top-right panel*) is scattered from the inner planet and gets *tossed* into an inner orbit with higher eccentricity (*top-left panel*). We see the planet is actually tossed close to the 2:1 resonance, but now with the smaller planet on the inside (*bottom-left panel*).

Another example is having planets get tossed into farther orbits. Figure 4.10 shows a 1 M_E planet becoming locked into a 5:4 resonance with a 1 M_J inner planet. However, initial eccentricities and the small orbital separation of the resonance caused the outer planet to be tossed farther out due to gravitational interactions with the inner planet. The planet, with initial eccentricities < 0.1, is tossed *into the 4:1 resonance* with eccentricities > 0.5! It is clear that this mechanism is crucial in creating the high eccentricities observed in planetary systems. Using *ResCap*, we will soon understand the frequency at which these phenomena can occur and will be able to characterize the significance of determining why we observe so many highly eccentric planets.

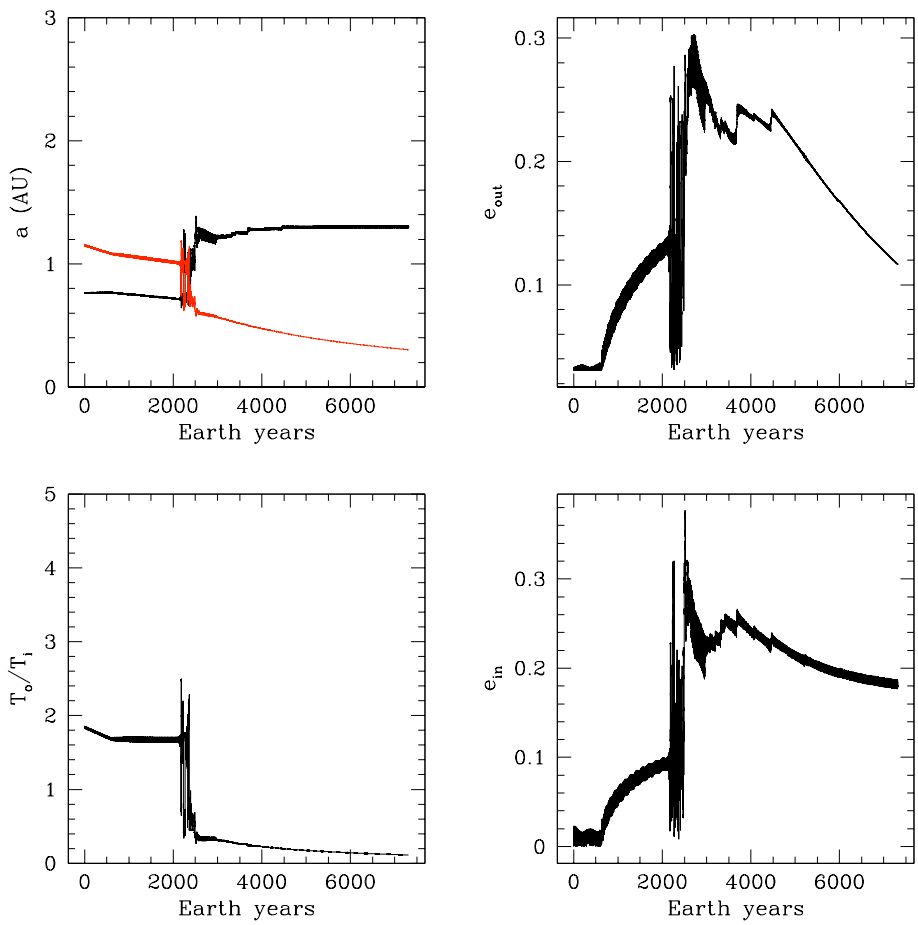

Figure 4.8: Two 1 M_J planets undergoing dynamical instability in the 3:2 resonance. In the end, as seen in the *top-left panel*, the planets switch places, leaving the (originally) inner planet with an eccentric orbit, as seen in the *bottom-right panel*.

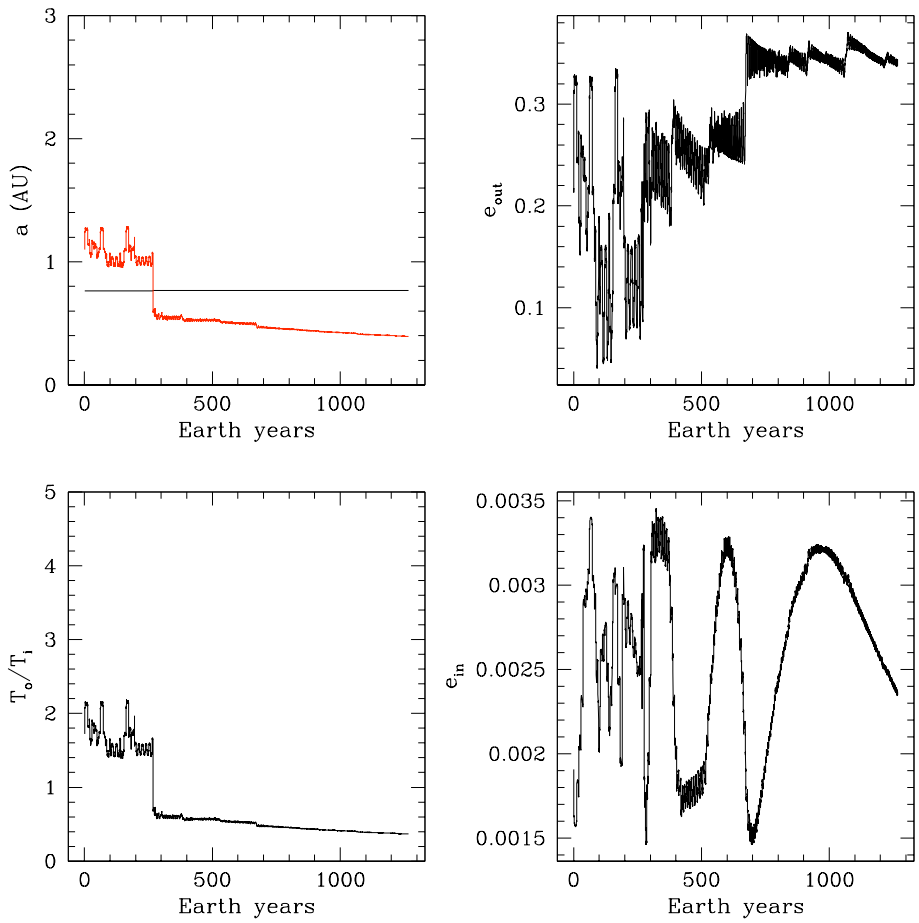

Figure 4.9: A 1 M_E planet being scattered into a 2:1 resonance from gravitational interactions with a 1 M_J planet.

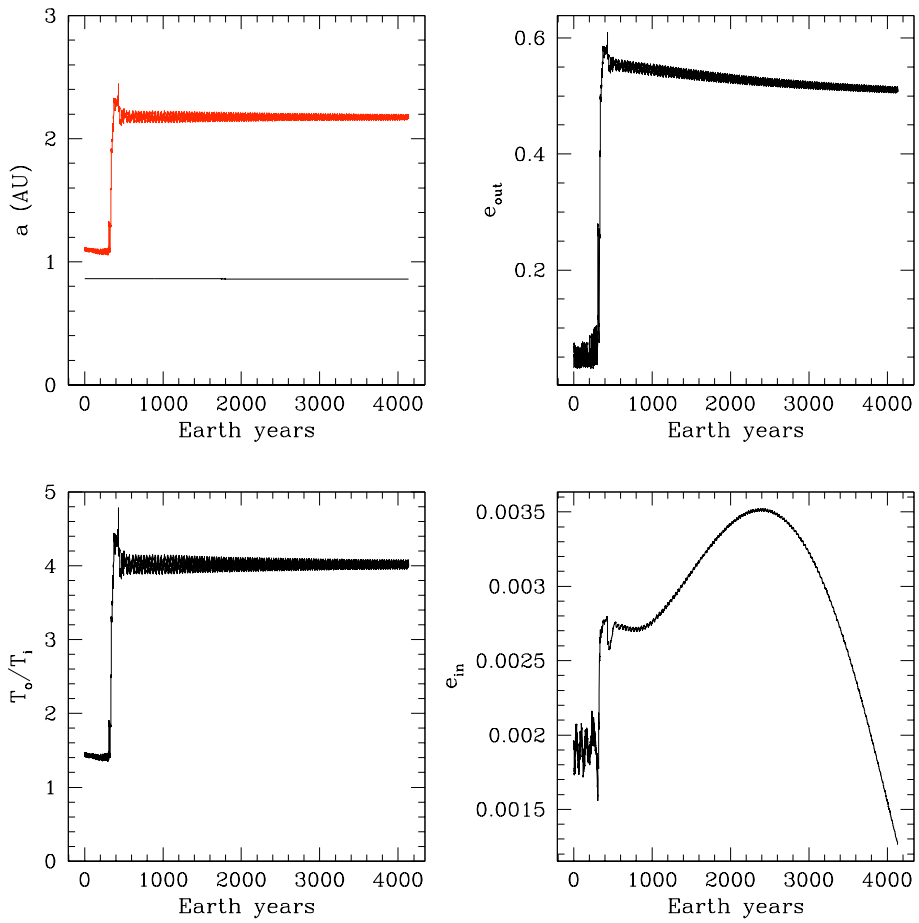

Figure 4.10: A 1 M_E planet being scattered into a 4:1 resonance with higher final eccentricities from gravitational interactions with a 1 M_J planet.

Chapter 5

Summary and Discussion

The recent observations of extrasolar planets strongly suggest that gravitational interactions between forming planets and the disc in which they are embedded are a key element in the understanding of planet formation. For example, theory suggests that planet-disc tidal interactions allow orbital migration to place hot Jupiters where we observe them today (Goldreich & Tremaine 1979, 1980; Lin & Papaloizou 1979, 1993).

A substantial amount of work has been done in the last decade to gain a stronger understanding of planet-disc tidal interactions. Three dimensional numerical simulations incorporating magneto hydrodynamic turbulence rather than anomalous viscosity prescriptions have begun and have shown magnetic interactions with the disc can strongly affect migration, especially in the Earth-mass range.

The results of this study are part of the pioneering steps to understand migration processes on a global level. We are currently at a point where we can study each stage of planet formation individually, but simulations taking into account all of these processes cannot be done. This would require very complex computations that cannot yet be performed on a reasonable timescale. Working toward the day when those simulations will be possible, this study has helped to better understand the following:

- The evolutionary outcome, i.e., final orbital configuration of the system, depends strongly on the properties of the protoplanetary disc and the initial conditions. Understanding which of these properties are important will allow us to predict the long-term evolution and stability of planetary systems without the need for massive numerical simulations.

- The presence of high orbital eccentricities amongst extrasolar planets is suggestive of a strong orbital relaxation or scattering process. For this to happen, formation must occur on a timescale short enough that dynamical interactions may take place subsequently. The gaseous environment of the disc appears to inhibit such interactions until it is removed.

Runaway migration is a problem facing current theories of planet formation: theory suggests that most planets should migrate into the star on timescales much shorter ($10^4 - 10^5$ yr) than the lifetime of the protoplanetary disc ($10^6 - 10^7$ yr). I find that when the planets' equations of motion take into account their coupling to the disc (Papaloizou & Larwood 2000), the lifetime of Earth-size planets trapped in mean motion resonances can be prolonged to the timescales of the protoplanetary disc. Disc coupling acts to increase the rate of migration, but the coupling between the orbit and the disc would be weaker for eccentric orbits due to the larger relative velocity of the planet and the local disc material. Therefore, small planets on eccentric orbits are fully decoupled from the disc are not subjected to the strong frictional forces that would drag the planet into the star. However, this does not help to prevent rapid migration for planets above a few Earth-masses. Further investigations including orbital inclination within a disc and N-body simulations (so to include scattering effects) will allow me to deduce the role this coupling and mean motion resonance have on preventing runaway migration.

By modeling the frictional effects of a protoplanetary disc through a migration term and an eccentricity damping term, I am able to create systems with planets both locked in mean motion resonance and with fixed eccentricities. By imposing the condition that the timescale for eccentricity damping is less than or equal to migration timescale, $a/\dot{a}$ (Goldreich & Tremaine 1980), I can build eccentricities up to ~ 0.6 from initially circular orbits. Further "fine tuning" of these parameters allow for the reproduction of characteristics in observed systems such as GJ 876 (Lee & Peale 2002). However, what is important is that resonance is a mechanism through which eccentric planets can be created, serving to help explain the statistical observation that over half of observed extrasolar planets have eccentricities above 0.2.

The probability for trapping into mean motion resonance depends on several characteristics of the system. I have shown that the mass ratio plays a substantial role in whether trapping occurs for first-order resonances. This is consistent with Peale's (2004) study of the 2:1 resonance, but extends the analysis to the general class of first-order resonances. Additionally, I have shown resonance trapping into second and third-order resonances requires some non-zero eccentricity. However, less than 5% of my simulations were able to produce these sort of resonances from migration alone; planet-planet scattering accounted for the majority ($> 70\%$) of second and third-order resonance captures.

Dynamical instabilities between two planets can produce the observed large eccentricities observed in extrasolar planetary systems. In these situations, one planet is either ejected or thrown into an orbit far from the dynamically unstable region. In either case, the surviving planets remain with highly eccentric orbits (Rasio & Ford 1996; Weidenschilling & Marzari 2001). I have shown this mechanism can produce planets locked in second or third-order resonances (e.g., 3:1 or 4:1), which are difficult to produce through migration alone. This planet-planet scattering provides very short timescales for both eccentricity growth and for removing the strong perturbations. This occurs because a planet is either ejected or the orbital separation between the planets becomes large.

Dynamical instability has additional implications for planet formation. The formation of hot Jupiters assumes the gas giants were formed farther out and migrated inward through torques applied by the protoplanetary disc (Goldreich & Sari 2003). However, if dynamical instabilities occurred after sufficient migration, the perturbing bodies could be discarded, and gas giants could be left on eccentric orbits close to their parent star. Further simulations of these unstable systems will allow for a statistical comparison between the outcomes and the currently observed distribution of eccentricities. Additionally, it will allow us to compare this theory of hot Jupiter formation to theories suggesting that the planets did indeed form near their current positions (Bodenheimer et al. 2000).

I am grateful for the support and guidance of my advisor, Professor Frederic Rasio. I would also like to acknowledge the help of Dr. Edward Thommes who, along with Professor Rasio, has made this project possible. This work was supported by NSF Grant AST–0507727 to Northwestern University.

Appendix A

List of Notation

Definition of Orbital Elements

semi-major axis, a **-** half the length of the longest distance between two points of the orbital ellipse

semi-minor axis - half the length of the shortest distance between two points of the orbital ellipse

eccentricity, e **-** equal to $\sqrt{1-(b/a)^2}$, where a and b are the semi-major and semi-minor exes of the orbital ellipse, respectively; thus $e = 0$ corresponds to a perfect circle, while $e = 1$ corresponds to a straight line

true anomaly, f **-** the angle between the line from the central star to the pericenter and the line from the central star to the planet

inclination, i **-** the angle between the plane of the orbit and the reference plane

argument of pericenter, ω **-** the angle between the line from the central star to the longitude of ascending node and the line from the central star to the pericenter

longitude of ascending node, Ω **-** the angle between the line from the central star to a reference direction and the line from the central star to the planet on the orbit where the planet crosses from below the reference planet to above the reference plane

longitude of pericenter, ϖ **-** equal to $\omega + \Omega$; note that this is a "dogleg" angle since ω lies in the orbital plane and Ω lies in the reference plane

time of pericenter passage, τ **-** the time at which the planet passes through the point on its orbit closest to the central star

mean anamoly, M **-** defined as $n(t-\tau)$, where n is the mean motion angular velocity

mean longitude, λ - defined as $M + \varpi$

General Notation Used

$M_\odot$ **-** a Solar-mass ($1.98892 \cdot 10^{30}$ kg)

M_J **-** a Jupiter-mass ($1.8987 \cdot 10^{27}$ kg)

M_E **-** an Earth-mass ($5.9742 \cdot 10^{24}$ kg $\sim 1/300\ M_J$)

G **-** the gravitational constant ($6.673 \cdot 10^{-11}$ $\mathrm{m^3\,kg^{-1}\,s^{-2}}$)

M_* **-** the mass of the central object in a three-body system

M_i **-** the mass of the inner planet in a three-body system

M_o **-** the mass of the outer planet in a three-body system

X_p **-** a characteristic of the planet, where X could be the radius (R), the mass (M), radial distance from the central star, etc.; the context will make it clear

α**,** β **-** dimensionless constants

Ω **-** the Keplerian angular velocity of an object orbiting a M_* star

Σ **-** the surface density of a protoplanetary disc

H **-** height of the protoplanetary disc

Notation Used in Chapter 1

F **-** the stellar flux from an observed star

Notation Used in Chapter 2

τ_e **-** grain velocity damping timescale

τ_s **-** grain sedimentation timescale

f **-** dimensionless constants except in equation 2.14, where f signifies the equation of friction

T **-** in this chapter T is the toque on an object

T_{vis} **-** the viscous torque on a planet embedded in a protoplanetary disc

T_{tide} **-** the tidal torque on a planet embedded in a protoplanetary disc

Notation Used in Chapter 3

$O(h^\beta)$ **-** encapsulates all terms of order h^β and higher

Δ **-** the truncation error

Δ_0 **-** the minimum allowed error per timestep in *ResCap*

h **-** the step size

ϕ **-** the map from (kg,m,s)-units to $(\tilde{M}, \tilde{L}, \tilde{T})$-units

$\Re$ **-** defined as $p/(p+q)$, where p and q are integers

f_i^j **-** the migration equation for the j-th body in the i-th direction

Notation Used in Chapter 4

f **-** the equation of friction

t_{mig} **-** the migration timescale

t_{ecc} **-** the eccentricity damping timescale

Δ **-** the width of the gap formed by the planet embedded in a protoplanetary disc

K **-** the ratio between $tmig$ and t_{ecc}

r_{Hill} **-** the Hill radius for a body M_i orbiting a central star

Appendix B

ResCap Source Code

The entire code is appended on the following pages. See comments within the code for further details than that presented in Chapter 3.

res.c - the main code the includes the parameters, initial conditions, differential equations, and flow mechanism of *ResCap*

The remaining code is adopted from Numerical Recipes (Press et al. 2002)

odeint.c - the fourth-order Runge-Kutta numerical integrator

nrutil.c ; nrutil.h - system files that control the flow of *ResCap* and error handling

rk4.c - fourth-order equations that gathers information necessary for the error-check program

rckc.c - error-check program measuring the truncation error

rkqs.c - step-size adjuster and step-advancement program

References

Alexander S G and Agnore C B 1998 *Icarus* **132** 113

Alonso R, et al. 2004 *Astrophys. J. Letters* **613** L153

Armitage P J & Hansen B M S 1999 *Nature* **402** 633

Artymowicz P 1992 *PASP* **679** 769

— 1993 *Astrophys. J.* **419** 166

— 2004 *Astr. Soc. Pac.* **324** 39

Bennett D P and Rhie S H 1996 *Astrophys. J.* **472** 660

Bodenheimer P et al. 2000 *Icarus* **143** 9

Bond I A, Udalski A, Jarcszyński M et al. 2004 *Astrophys. J.* **606** L155

Bonnell I A, Bate M R, Clarke C J & Pringle J E 1997 *MNRAS* **285** 201

Boss A P 2006 *Astrophys. J.* **643** 501

Boss A P & Durisen R H 2005 *Astrophys. J. Letters* **621** L137

Bryden G Rózyczka M Lin D N C & Bodenheimer P 2000 *Astrophys. J.* **540** 1091

Cameron A G W 1978 *Moon Planets* **18** 5

Cash J R and Karp A H 1990 *ACM Transactions on Mathematical Software* vol. 16

Chaing E I, Fischer D and Thommes E *Astroph. J. Letters* **564** L105

Chambers J E 1999 *MNRAS* **304** 793

Charbonneau D, Brown T M, Latham D W and Mayor M 2000 *Astrophys. J. Letters* **529** L45

Deming D, Seager S, Richardson L J and Harrington J *Nature* 2005 **434** 740

Drazin P G, Reid W H 1981 *Hydrodynamic Stability* (Cambridge: Cambridge University Press) p 69

Fehlberg E 1969 *NASA Technical Report* 315

Goldreich P 1965 *Mon. Not. R. Astron. Soc.* **130** 159

Goldreich P and Ward W R 1973 *Astrophys. J.* **183** 1051

Goldreich P and Sari R 2003 *Astrophys. J.* **585** 1024

Goldreich P and Tremaine S 1979 *Astrophys. J.* **233** 857

— 1980 *Astrophys. J.* **241** 425

Gould A and Loeb A 1992 *Astrophys. J.* **396** 104

Kley W 2000 *MNRAS* **313** L47

— 2003 *CeMDA* **87** 85

Kuiper G P 1949 *Astrophys. J.* **109** 308

Lee M H 2004 *Astrophys. J.* **611** 517

Lee M H and Peale S J 2002 *Astrophys. J.* **567** 596

Lin D N C 1997 *Proc. IAU Colloq. 163: Accretion phenomena and related outflows* ASP Conf. Series vol 121 ed D T Wickramasinghe et al. (San Francisco: ASP) p 321

Lin D N C, Bodenheimer P and Richardson D C 1996 *Nature* **380** 606

Lin D N C, and Papaloizou J C B 1979 *Mon. Not. R. Astron. Soc.* **186** 799

— 1986 *Astrophys. J.* **309** 846

— 1993 *Protostars and Planets III* ed E H Levy and J I Lunine (Tuscon: University of Arizona Press) p 749

Lin D N C Papaloizou J C B 1993 in *Protostars and Planets III* eds. E H Levy and J I Lunine (Tuscon: Univ. of Arizona Press), 749

Lin D N C, Papaloizou J C B, Terquern C, Bryden G and Ida S 2000 *Protostars and Planets IV* ed V. Mannings et al. (Tucson: University of Arizona Press) p 1111

Lissauer, J J 1993 *Ann Rev Astron Ap* 31 129

— 1995 *Icarus* **114** 217

Lufkin G, Quinn T, Wadsley J, Stadel J, & Governato F 2004 *MNRAS* **347** 421

Lynden-Bell D, Pringle J E 1974 *MNRAS* **168** 603

Malhotra R 1993 *Nature* **365** 819

– 2003 *Astroph. J. Letters* **573** L33

Marcy G W and Butler R P 1995 *187th AAS Meeting BAAS* vol 27 p 1379

Marcy G W, Butler R P, Fischer D, Vogt S S, Lissauer J J and Rivera E J 2001 *Astrophys. J.* **556** 296

Marcy G W, Butler R P, Fischer D, Vogt S S, Wright J T, Tinney C G and Jones H R A 2005 *Astrophys. J.* ???

Mao S and Paczynski B 1991 *Astrophys. J. Letters* **374** L37

Marzari F & Weidenschilling S J *Icarus* **156** 570

Masset F and Papaloizou J C B 2003 *Astrophys. J.* **588** 494

Mayor L et al. *Astrophys. J. Letters* **661** L77

Mayor M and Queloz D 1995 *Nature* **378** 355

Mizuno H 1980 *Prog Theor Phys* **96** 266

Murray N, Hansen B, Holman M and Tremaine S 1998 *Science* **279** 69

Papaloizou J C B and Larwood J D 2000 *MNRAS* **315** 823

Papaloizou J C B Nelson R P & Masset F 2001 *A&A* **366** 263

Pollack J B Hubickyj O Bodenheimer P Lissauer J J Podolak M Greenzweig Y 1996 Icarus **124** 62

Press et al. 2002 *Numerical Recipes in C: Second Edition* Cambridge University Press, New York, New York

Quillen A C 2006 *Mon. Not. Roy. Astron. Soc.* **365** 1367

Rasio F A and Ford E B 1996 *Science* **274** 54

— 2007 *Submitted to ApJ*

Safronov V S 1969 English translation 1972 *Evolution of the protoplanetary cloud and formation of the Earth and planets* (IPST Jerusalem)

Shakura N I and Sunysev R A 1973 *Astron. Astrophys.* **24** 337

Thommes E 2005 *Astrophys. J.* **626** 1033

Udry S, Mayor M and Santos N C 2003 *Astron. Astrophys.* **407** 369

Vidal-Madjar A, et al. 2004 *Astrophys. J* **604** L69

Vidal-Madjar A, Lecavelier des Etangs A, Désert J M, Ballester G E, Ferlet R, Hébrard G and Mayor M 2003 *Nature* **422** 143

Ward W R 1986 *Icarus* **67** 164

Ward W R 1997 *Icarus* **126** 261

Weidenschilling S J 1977 *Mon. Not. R. Astron. Soc.* **180** 57

Weidenschilling S J and Marzari F 1996 *Nature* **384** 619

Wisdom J and Holman M 1991 *Astrophys. J.* **102** 1528

Wu Y and Murray N 2003 *Astrophys. J.* **589** 605